EPRI | ELECTRIC POWER RESEARCH INSTITUTE

Magnetohydrodynamic Electromagnetic Pulse Assessment of the Continental U.S. Electric Grid

Geomagnetically Induced Current and Transformer Thermal Analysis

3002009001

Magnetohydrodynamic Electromagnetic Pulse Assessment of the Continental U.S. Electric Grid

Geomagnetically Induced Current and Transformer Thermal Analysis

3002009001

Technical Update, February 2017

EPRI Project Manager

R. Horton

ELECTRIC POWER RESEARCH INSTITUTE
3420 Hillview Avenue, Palo Alto, California 94304-1338 ▪ PO Box 10412, Palo Alto, California 94303-0813 ▪ USA
800.313.3774 ▪ 650.855.2121 ▪ askepri@epri.com ▪ www.epri.com

DISCLAIMER OF WARRANTIES AND LIMITATION OF LIABILITIES

THE FOLLOWING ORGANIZATIONS PREPARED THIS REPORT:

PowerWorld Corporation

Walling Energy Systems Consulting, LLC

Electric Power Research Institute (EPRI)

This is an EPRI Technical Update report. A Technical Update report is intended as an informal report of continuing research, a meeting, or a topical study. It is not a final EPRI technical report.

NOTE

For further information about EPRI, call the EPRI Customer Assistance Center at 800.313.3774 or e-mail askepri@epri.com.

ACKNOWLEDGMENTS

The following organizations prepared this report:

PowerWorld Corporation
2001 South First Street
Champaign, IL 61820

Principal Investigators
S. Dahman
T. Overbye

Walling Energy Systems Consulting, LLC
438 Vischer Ferry Road
Clifton Park, NY 12065

Principal Investigator
R. Walling

Electric Power Research Institute (EPRI)
3420 Hillview Avenue
Palo Alto, CA 94303

Principal Investigator
R. Horton

This report describes research sponsored by EPRI.

This publication is a corporate document that should be cited in the literature in the following manner:

Magnetohydrodynamic Electromagnetic Pulse Assessment of the Continental U.S. Electric Grid: Geomagnetically Induced Current and Transformer Thermal Analysis. EPRI, Palo Alto, CA: 2017. 3002009001.

ABSTRACT

The high-altitude detonation of a nuclear weapon can generate a large electromagnetic pulse (referred to as a high-altitude EMP or HEMP) that is comprised of three components: E1, E2 and E3. Depending on weapon yield and height of burst the resulting EMP can impact a large geographical area. E1 and E2, which can result in damage to electronic components and low and medium voltage electric infrastructure, refer to the nearly-instantaneous emissions that are most commonly associated with HEMP. The latter component, E3, or magnetohydrodynamic electromagnetic pulse (MHD-EMP) can drive low frequency, geomagnetically-induced currents (GIC) in transmission lines and power transformers which can result in voltage collapse and increased hotspot heating in bulk-power transformers. The potential impact of MHD-EMP on hotspot heating in bulk-power system transformers located in the portion of the grid affected by a high-altitude detonation is of particular importance, and was the focus of this work.

The following report describes the methodology, models and results of an assessment that was performed on the United States transformer fleet to determine the potential for widespread transformer damage resulting from MHD-EMP (E3) from a single high-altitude burst over the Continental United States (CONUS). While the analysis undertaken used state-of-the-art modeling and analysis techniques, uncertainties related to modeling parameters derived from readily-available data and the nature of the MHD-EMP (E3) environment required that assumptions be made. These assumptions and their implications have been documented throughout the report such that the results obtained can be used to inform mitigation strategies as well as future assessments to determine the overall bulk-power system reliability impacts of MHD-EMP (E3).

Based upon our analysis, a small number of geographically dispersed transformers were found to be at potential risk of thermal damage from MHD-EMP (E3) generated by a single high-altitude burst over the CONUS. Although it was determined that a relatively small number of transformers would be at potential risk of thermal damage and their locations were geographically dispersed, it is important to note that the potential impact of the loss of these transformers, should any of them experience thermal damage, was not considered in this study. Future research activities identified as a part of this study will attempt to improve our understanding of the overall system reliability impacts of experiencing damage to a small number of bulk-power transformers over a large area such as an electrical interconnection.

Keywords
Bulk-power system
Electromagnetic pulse (EMP)
Geomagnetic disturbance
High-altitude electromagnetic pulse (HEMP)
Magnetohydrodynamic electromagnetic pulse (MHD-EMP)

Deliverable Number: 3002009001

Product Type: Technical Update

Product Title: Magnetohydrodynamic Electromagnetic Pulse Assessment of the Continental U.S. Electric Grid: Geomagnetically Induced Current and Transformer Thermal Analysis

PRIMARY AUDIENCE: Asset Owners and Operators of the United States Bulk-Power System

SECONDARY AUDIENCE: Regulators, State and Federal Entities

KEY RESEARCH QUESTION

This study was performed to determine the potential for a significant number (hundreds) of bulk-power transformers to experience thermal damage caused by the geomagnetically-induced current (GIC) flows generated by a single high-altitude nuclear burst over the Continental United States (CONUS). The research sought to reconcile opposing conclusions presented in earlier research performed by Oak Ridge National Laboratories (ORNL) in the mid-late 1980's and Metatech in late 2000's related to the effects of magnetohydrodynamic electromagnetic pulse (MHD-EMP, E3) on bulk-power system transformers.

RESEARCH OVERVIEW

This research evaluated the potential impacts of E3 on bulk-power system transformers. The fundamental approach to this study was similar to that adopted by the North American Electric Reliability Corporation (NERC) to assess the potential impacts of severe geomagnetic disturbance (GMD) events on bulk-power transformers. First, the electric field environment necessary for calculating GIC flows was identified and a dc model of the interconnection-wide system was assembled. For this study, a publicly available MHD-EMP (E3) environment along with a model of the United States bulk electric system was used to calculate the GIC flows in the transmission system that would result from a single, high-altitude detonation over the CONUS. GIC calculations were then performed assuming 11 different target locations. The resulting time-series GIC flows were then used to compute the time-series hotspot temperature of each bulk-power system transformer included in the interconnection-wide assessment. The maximum instantaneous hotspot temperatures were then evaluated against conservative temperature limits that were based on an assumed condition-based GIC susceptibility category of the entire transformer fleet. The number of transformers that were identified as exceeding the specified temperature limits were then combined with the probabilities of a given transformer being in one of the three specified categories to estimate the number of bulk-power transformers to be at potential risk of thermal damage. Additionally, the potential for thermal damage caused by circulating harmonic currents in the tertiary windings of large autotransformers was also evaluated.

KEY FINDINGS

- Although a significant number of transformers (hundreds to thousands) could experience GIC flows greater than or equal to 75 amps/phase (screening criteria adopted from NERC TPL-007-1), only a small number (3 to 14 depending on the target location evaluated) of these transformers were found to be at potential risk of thermal damage. In addition, the at-risk transformers were found to be geographically dispersed.
- Assessment results also indicate that damaging levels of tertiary winding heating resulting from the flow of harmonic currents generated by the resulting GIC flows are unlikely to occur.

WHY THIS MATTERS

Results of prior assessments performed to determine the impacts of E3 on bulk-power transformers range from transformer damage from E3 is unlikely[1] to up to 100 transformers could be at potential risk of thermal damage[2]. The results of this study provide a strong technical basis for reconciling these opposing conclusions.

HOW TO APPLY RESULTS

The results of this study are in agreement with earlier work performed by ORNL which indicate that the failure of a large number (hundreds) of bulk-power transformers from E3 is unlikely. The assessment results can be used to help quantify the overall risk of E3 impacting the bulk-power system as a whole (interconnection-level assessment), but should not be interpreted to indicate E3 will not affect bulk-power reliability since the potential for widespread outages due to voltage collapse or the synergistic effects of E1, E2 and E3 are still being investigated. Additionally, because of the number of conservative assumptions that were required due to the lack of asset specific data, the results should not be used to inform investment decisions at individual utilities.

EPRI CONTACTS: Randy Horton, Senior Technical Executive, rhorton@epri.com

PROGRAM: P37 - Substations

[1] "Impacts of a Nominal Nuclear Electromagnetic Pulse on Electric Power Systems – Phase III – Final Report," *Oak Ridge National Laboratory (ORNL),* ORNL/Sub-83/43374/2/April 1991.

[2] "Meta-R-321, The Late-Time (E3) High-Altitude Electromagnetic Pulse (HEMP) and Its Impact on the U.S. Power Grid," *Metatech Corporation,* January 2010, https://www.ferc.gov/industries/electric/indus-act/reliability/cybersecurity/ferc_executive_summary.pdf.

Electric Power Research Institute
3420 Hillview Avenue, Palo Alto, California 94304-1338 • PO Box 10412, Palo Alto, California 94303-0813 USA
800.313.3774 • 650.855.2121 • askepri@epri.com • www.epri.com

CONTENTS

LIST OF FIGURES

LIST OF TABLES

1
INTRODUCTION

Background and Motivation for This Research

The high-altitude detonation of a nuclear weapon can generate a large electromagnetic pulse (EMP), referred to as a high-altitude EMP (HEMP). The resulting electromagnetic pulse is composed of three components: E1, E2, and E3. E1 and E2 refer to the nearly instantaneous emissions that are most commonly associated with HEMP and damage to electronic components and low- and medium-voltage electric infrastructure. The last component, E3, or magnetohydrodynamic electromagnetic pulse (MHD-EMP) can drive low-frequency, geomagnetically induced currents (GICs) in transmission lines and power transformers that can result in half-cycle saturation of power transformers that can lead to 1) voltage collapse as a result of increased reactive power consumption and misoperation of protection systems due to harmonics and 2) additional hotspot heating in bulk-power transformers. The potential impact of the resulting GIC on hotspot heating in bulk-power transformers is of interest. Because of the potential impact of MHD-EMP (E3) on the bulk-power system, concern has been raised by some stakeholders that a HEMP attack on the U.S. power grid could potentially result in a blackout that could last several months or longer [1, 2]. Such a scenario is based on the assumed failure of a significant number of large power transformers by MHD-EMP (E3) which could take an extended period to replace based on the number of available spares and procurement time of additional replacements [1].

To address the concern of potential damage caused by a HEMP attack, several studies have been performed over the last 30 years to determine the impacts of MHD-EMP (E3) on the bulk-power system [3, 4, 5]. However, the modeling techniques and methods used to perform the assessments vary considerably. Consequently, the results of these prior studies vary as well. Since the time that the assessments described in [3, 4, 5] were carried out, there have been improvements made with regard to modeling the impacts of GIC on the bulk-power system and its components. For example, time-domain thermal models that consider both the magnitude and duration of GIC flow in transformers have been developed [6]. In addition, such modeling improvements have yet to be incorporated in a large-scale MHD-EMP (E3) assessment. Therefore, the principal motivation for this research was to improve the accuracy of prior assessments by including the latest scientific advancements relative to modeling power system impacts resulting from GIC flows induced by MHD-EMP (E3).

Objective

The primary objective of this study was to determine the potential for widespread failure of bulk-power transformers resulting from thermal damage caused by MHD-EMP (E3) from a single, high-altitude burst over the Continental United States (CONUS).

Scope

The scope of this study was restricted to assessing the potential impacts of MHD-EMP (E3) on the bulk-power system transformers located in the CONUS. All bulk-power system transformers included in the United States portions of each of the major North American synchronous, interconnected power-grid models, that is, the Eastern Interconnection (MMWG), the Western Interconnection (WECC), and the Texas Interconnection (ERCOT), were included in the analysis. Using readily available data and state-of-the-art modeling and analysis techniques, the number of transformers that would be expected to be at potential risk of thermal damage caused by the GIC generated by MHD-EMP (E3) from a single, high-altitude burst over the CONUS was estimated.

Approach

The fundamental approach to this study was similar to the one described in North American Electric Reliability Corporation (NERC) TPL-007-1 Standard [7] and used to assess the potential impacts of severe geomagnetic disturbance (GMD) events. First, the electric field environment necessary for calculating GIC flows was identified, and a dc model of the interconnection-wide system was assembled. For this study, a publicly available MHD-EMP (E3) environment (refer to Section 2) along with a model of the United States bulk electric system was used to calculate the GIC flows in the transmission system that would result from a single, high-altitude detonation over the CONUS. GIC calculations were then performed assuming 11 different target locations. The resulting time-series GIC flows were then used to compute the time-series hotspot temperature of each bulk-power system transformer included in the interconnection-wide model. Each interconnection that was potentially affected by the MHD-EMP (E3) generated by the high-altitude nuclear detonation was evaluated independently. The maximum instantaneous hotspot temperatures were then evaluated against conservative performance criteria (that is, temperature limits) that were based on an assumed condition-based GIC susceptibility category of the entire transformer fleet. The number of transformers that were identified as exceeding the specified temperature limits were then combined with the probabilities of a given transformer being in one of the three specified categories to determine the estimated number of bulk-power transformers to be at potential risk of thermal damage. In addition, the potential for thermal damage caused by circulating harmonic currents in the tertiary windings of large autotransformers was also evaluated.

Although the analysis undertaken used state-of-the-art modeling and analysis techniques, uncertainties arising from the lack of specific data for all components in the model, deriving modeling parameters from available data and the nature of the MHD-EMP (E3) environment, required that assumptions be made. These assumptions and their implications are documented throughout the report such that the results obtained can be used to inform mitigation strategies as well as future assessments to determine the overall bulk-power system reliability impacts of MHD-EMP (E3).

2
GEOMAGNETICALLY INDUCED CURRENT MODEL AND MAGNETOHYDRODYNAMIC ELECTROMAGNETIC PULSE (E3) ENVIRONMENT

Overview

This section describes the following:

- The modeling approach that was used to calculate time-series GIC flows
- Modeling parameters and assumptions used in the GIC calculations
- The MHD-EMP (E3) environment that was selected for this study

Modeling Approach

The modeling approach used to compute GIC flows resulting from MHD-EMP (E3) is illustrated in Figure 2-1.

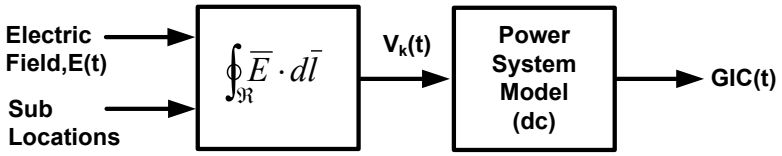

Figure 2-1
Simplified flowchart of the modeling approach used to compute geomagnetically induced current flows generated by magnetohydrodynamic electromagnetic pulse (E3)

The fundamental approach used in this study to calculate GIC was similar to the one described in NERC TPL-007-1 Standard [7] and used to assess the potential impacts of severe GMD events. First, the electric field environment including spatial and temporal characteristics was defined and used as the input to the assessment process. For this study, a publicly available MHD-EMP (E3) environment resulting from a single, high-altitude detonation over the CONUS was used (refer to subheading "Magnetohydrodynamic Electromagnetic Pulse (E3) Environment" in this section). Next, a dc model, including the locations of all of the substations and generating stations, was assembled for each of the three interconnection-wide models. Using the MHD-EMP (E3) environment and the substation locations, the induced voltages resulting from the coupling of the MHD-EMP (E3) signal with the transmission lines was determined. The resulting induced voltages were then combined with a dc model of the bulk-power system to compute the GIC in all transmission lines and bulk-power transformers in the interconnection. The analysis was performed for 11 target locations in the CONUS. Each interconnection that was potentially affected by the MHD-EMP (E3) generated by the high-altitude nuclear detonation over a given target location was evaluated independently.

Geomagnetically Induced Current Calculations

The GIC calculations performed in this study followed the procedures accepted by the NERC and described in [8, 9]. The MHD-EMP (E3) environment that is generated by a single, high-altitude nuclear burst was modeled as a time-varying, non-uniform electric field superimposed on the interconnection-wide grid model. At each instance in time, the effect of the electric field on each transmission line k was modeled as a dc voltage source, V_k, in series with the line's resistance. The value of this dc voltage was determined by integrating the electric field along the path of the transmission line:

$$V_k = \oint_{\Re} \overline{E} \cdot d\overline{l} \qquad \textbf{Eq. 2-1}$$

Where:

$\mathcal{R}$ is the geographic route of transmission line k
$\overline{E}$ is the electric field along this route (magnitude and direction)
$d\overline{l}$ is the incremental line segment (magnitude and direction)

If the electric field were uniform, this integration would be path independent. However, in the case of non-uniform electric fields such as those considered in this study, the integration depends on the transmission line's route between substations. Because the transmission line routes were unknown, a straight-line path was assumed. To account for the spatially varying electric field, the integration was performed by dividing the transmission line into segments no larger than 10 km in length and assuming the electric field was constant over each segment. The magnitude of the electric field was set to the value at the midpoint of each segment. Because of the relatively modest variation in the electric field over each 10-km line segment, the error introduced by this approach is considered negligible.

Next, to understand how the induced voltages were used to calculate the GICs, consider a standard m bus power flow model (that is, positive-sequence model) in which the m buses are grouped into s substations; let $n = m + s$. Because the GICs at each instant in time are considered dc, how they flow through the power grid can be determined by solving:

$$\widetilde{V} = [G]^{-1}\widetilde{I} \qquad \textbf{Eq. 2-2}$$

where $[G]$ is an n by n symmetric matrix similar in form to the m by m power system bus admittance matrix, except [10]:

- It is a real matrix with just conductance values.
- The conductance values are determined by the parallel combination of the three individual phase resistances for all power system devices.
- $[G]$ is augmented to include the substation neutral buses and substation grounding resistance values; hence, the order of the matrix is increased to n by n.

- Transmission lines with series capacitive compensation are omitted because series capacitors block the flow of GIC.
- The transformers are modeled with their winding resistance to the substation neutral and, in the case of autotransformers, both the series and common windings are represented explicitly.

The vector $\tilde{I}$ models the effect of the induced voltages in the transmission lines as a Norton equivalent circuit. For large systems, [*G*] is quite sparse, and hence, Equation 2-2 can be solved with computational effort equivalent to a single power flow iteration. When solved, the voltage vector $\tilde{V}$ contains entries for the *s* substation neutral dc voltages and the *m* bus dc voltages. From $\tilde{V}$, the GICs can be calculated for any power system element. An illustration of this approach is shown in Figure 2-2. Note that while dependent on transmission system topology and parameters (including the substation resistance), the GICs themselves are independent of the power system operating point. Therefore, the GIC calculations can be decoupled from the power flow analysis.

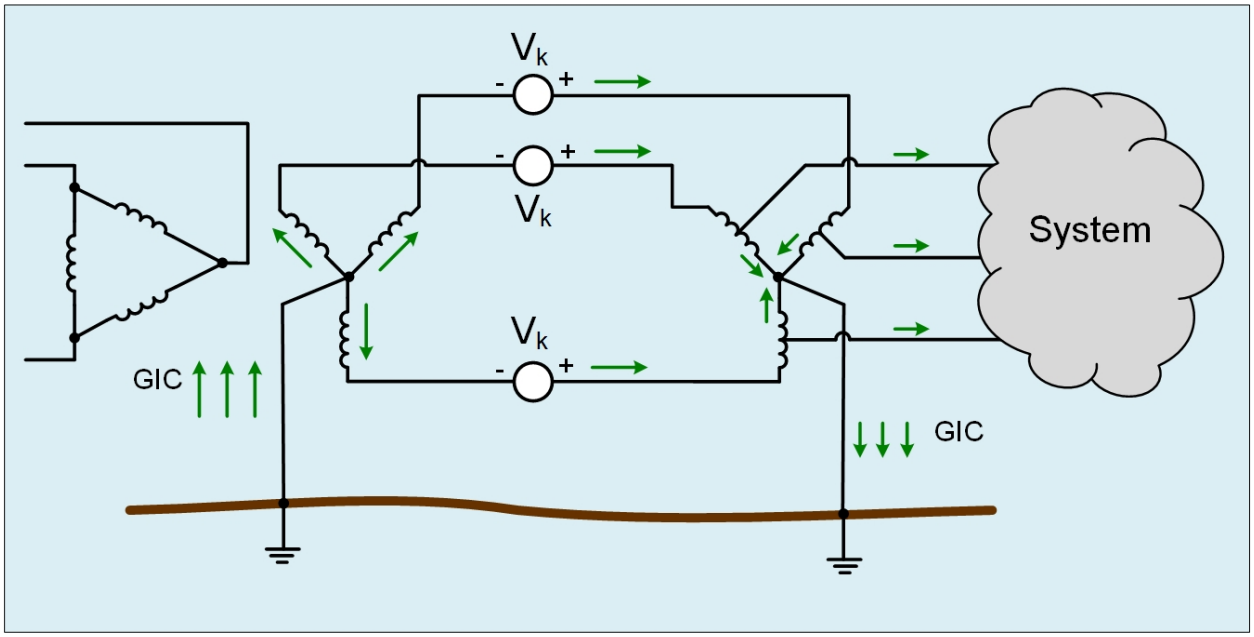

Figure 2-2
Simple geomagnetically induced current flow example

Lastly, the **effective** GIC, that is, the level of GIC that results in an offset flux in the transformer core leading to half-cycle saturation, was determined using the calculated GIC flows in the transformer windings. This study used the approach described in [11] for calculating the effective GIC in conventional transformers and autotransformers.

Dc Modeling Parameters

The power system models, or cases, were taken from Federal Energy Regulatory Commission (FERC) Form 715 filings for each of the major North American synchronous interconnected power grids:

- The Eastern Interconnection (MMWG)
- The Western Interconnection (WECC)
- The Texas Interconnection (ERCOT)

These cases provide real and reactive power flows for hypothetical summer peak conditions. They include electrical models of most major ac transmission lines and transformers with nominal voltages between 69 and 765 kV, major high-voltage dc transmission lines, power generating stations, and loads aggregated at transmission buses.

The file names and internal descriptions for each of the cases that were used in the study are as follows:

- MMWG_2017SUM_2015Series_Final: 2015 Series, ERAG/MMWG Base Case Library (CEII); 2017 Summer Peak Load Case, Final
- 16HS3a: Western Electricity Coordinating Council; 2016 HS3 Operating Case; October 20, 2015
- 15DSB_2017_SUM1_Final_10152014: 15DSB-2017 Sum On-Peak Base Case - Economic - ERCOT SSWG Final - ERCOT PSSE V3340 Mod V8002

Because the FERC 715 power flow models are intended primarily to study ac operation of the power system, they do not contain all of the necessary parameters required to calculate the GIC generated by MHD-EMP (E3). As such, several assumptions were made as a part of the analysis. The following sections provide a brief description of the assumptions that were made with regard to the transmission lines, transformers, and substations that were included in the interconnection-wide dc models that were used to calculate the GIC flows.

Transmission Lines

All 69 kV and above transmission lines provided in the FERC 715 power flow models were included in the dc network used to compute GIC flows. Each transmission line was modeled using the positive-sequence resistance values provided in the FERC 715 power flow model. Because no information regarding wire size, bundling, or assumed conductor temperature was provided, a determination regarding the potential changes in conductor resistance that result from skin effect or operating temperature could not be made. Reference [12] states that the correction factor for skin effect varies between 0.95 for large conductors (for example, 1590 MCM) and 1.00 for smaller conductors (below 750 MCM); however, these reduction factors are based on an operating temperature of 25°C. At higher operating temperatures, the conductor resistance increases significantly. For example, the ac resistance of 1590 MCM ACSR at 100°C is approximately 133% larger than the dc value at 25°C. Therefore, the positive-sequence values provided in the FERC 715 power flow models can be used as a conservative proxy for the dc resistance of the lines.

Transformers

All 69 kV and above bulk-power system transformers included in the FERC 715 power flow models were included in the dc network model. Key transformer parameters for GIC modeling include the following:

- Winding configuration and grounding
- dc winding resistance
- Transformer type (for example, autotransformer or conventional)

For this study, no specific parameters were provided by transmission and generation owners. Rather, the following assumptions were applied based on data available in the interconnection-level models considered here.

For this analysis, all transformer windings were assumed to be connected either delta or grounded wye. If the bus voltage that the high-voltage winding was connected to was greater than 300 kV and the bus voltage that the low-voltage winding was connected to was less than 100 kV, it was assumed the transformer was a generator step-up unit (GSU) with high side connected grounded wye and the low side connected delta. If the high side voltage was 100 kV or above and the low side had generation connected, the transformer was also assumed to be a GSU with winding connections defined previously. If the high side voltage was 100-299.9 kV and the low side did not have generation connected, then the transformer was treated as a load serving transformer with high side connected delta and low side connected grounded-wye. Because of the high side delta connection, load serving transformers are not subjected to the flow of GIC, and thus were excluded in the dc model. If the high- and low-voltage windings were both less than or both greater than 100 kV, both windings were assumed to be grounded wye. Transformers were assumed to be autotransformers if the following criteria were met:

- The transformer was not a phase-shifting transformer.
- The high side and low side were at different nominal voltages.
- The high-side nominal voltage was at least 100 kV.
- The turns ratio was less than or equal to 4.

For the interconnection-scale models considered in this study, estimates were required for the transformer dc winding resistances. Because the individual winding resistances were not available, the values needed to be derived from the positive-sequence ac per-unit series resistance in the power flow model. The value in the power flow model contains the total series ac resistance for both high- and low-voltage windings. One-half of the resistance was assigned to each transformer winding as recommended by NERC [8] and [9] when specific transformer test data are not available.

Substations

Key substation parameters are geographic location (that is, GPS coordinates) and the resistance of the substation ground grid including the effects of shield wires or grounded neutral wires that may be connected directly to the grid. The geographic locations of each of the substations were added to the models from external databases. Measured substation grounding resistance values were not provided for this study, and therefore, all substations were assumed to have

conservative grounding resistances of 0.1 ohms. For comparison and parameter sensitivity analysis, some computations were also performed with assumed substation grounding resistance of 0.3 and 0.5 ohms. The results demonstrated that the 0.1 ohm assumption for the substation grounding resistance yields higher GIC flows, and therefore, is conservative.

Magnetohydrodynamic Electromagnetic Pulse (E3) Environment

The MHD-EMP (E3) environment used in this assessment is based on the environment described in [4] and [5], and includes both blast- and heave-driven (E3A and E3B) components. The peak amplitude of the resulting electric field is approximately 24 V/km and is based on a conservative soil conductivity value of 0.001 S/m [4]. The MHD-EMP (E3) environment was modeled using the approach from [5] and [13], as the product of three independent terms:

$$\overline{E}\left(x, \mathrm{y}, \mathrm{t}\right) = \varepsilon(x, y)\, \overline{e}(\mathrm{x}, \mathrm{y})\, f(t) \qquad \textbf{Eq. 2-3}$$

Where:

ε(x,y) represents the spatially varying, time-invariant magnitude of the electric field at a location defined by coordinates x and y
$\overline{e}(\mathrm{x}, \mathrm{y})$ is a unit vector providing the direction of the electric field at a location defined by coordinates x and y
$f(t)$ is a time-varying, spatially-independent time scalar.

Note that different ε(x,y) and $\overline{e}(\mathrm{x}, \mathrm{y})$ were used during the E3A and E3B time periods. The $f(t)$ function was common to both periods and was modeled using the waveform shown in Figure 2-3.

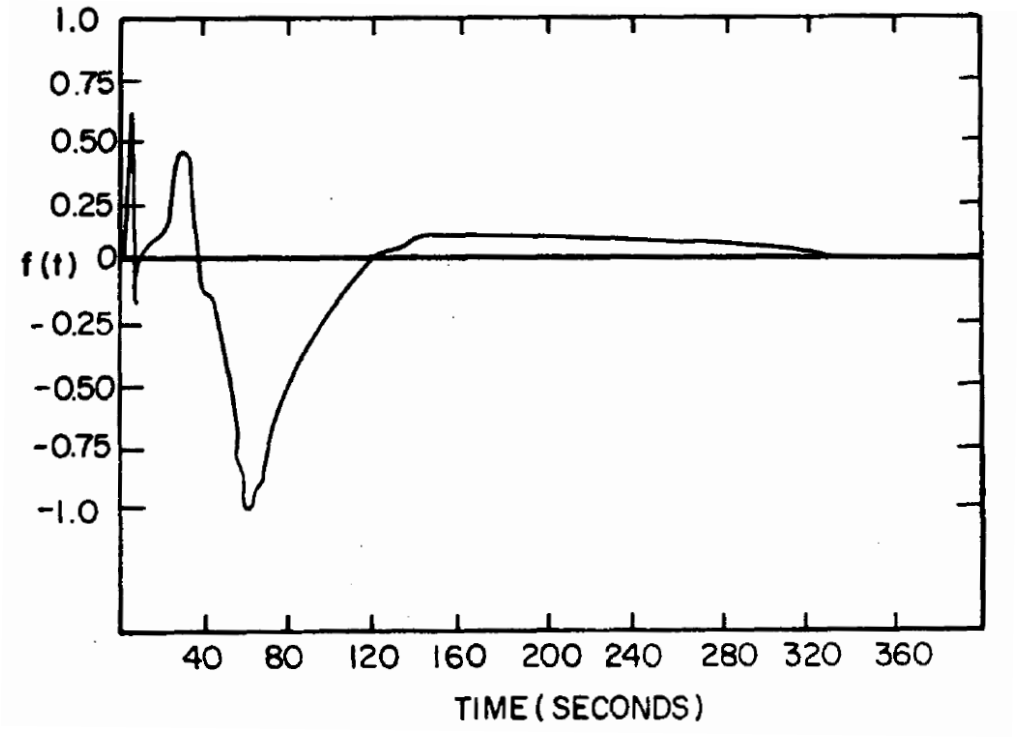

Figure 2-3
Magnetohydrodynamic electromagnetic pulse (E3) time-variation function, f(t)

Source: ORNL/Sub-83/43374/1/V3 [4]

Referring to Figure 2-3, the E3A component represents the first 10 seconds of the waveform, while the second component, E3B, begins at approximately 10 seconds and continues for the duration of the event, which is approximately five minutes.

E3A: Blast Wave

Based on the blast-driven component of the MHD-EMP (E3) environment described in [5] and illustrated in Figure 2-4, it was assumed during the E3A period that the magnitude of the electric field was uniform over a very large area (for example, CONUS region) with primarily east-west orientation.

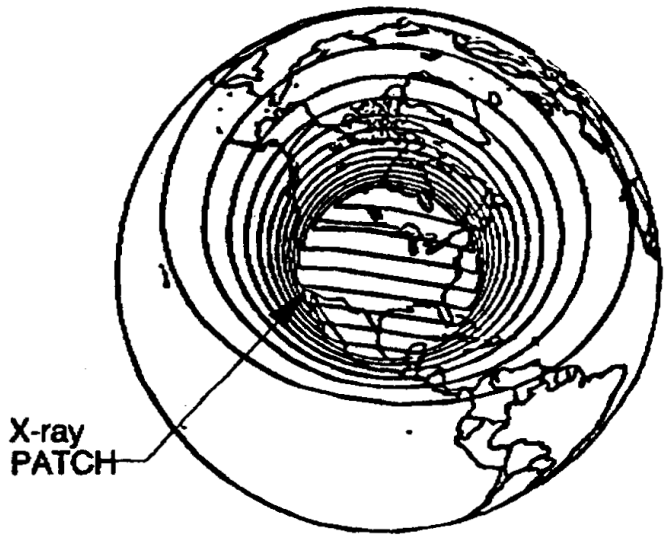

Figure 2-4
Notional illustration of the electric field lines of the E3A pulse for a detonation over the Central United States

Source: ORNL-6708 [5]

During the E3A period, the electric field across a given interconnection model was assumed to have uniform magnitude and direction. The magnitude of the E3A electric field varied with time as illustrated in Figure 2-3; however, the orientation remained fixed throughout the 10-second period associated with E3A. Because the peak magnitude of the MHD-EMP (E3) signal was 24 V/km (which occurs at approximately 60 seconds after detonation during the E3B period), the peak of the E3A electric field was approximately 14.4 V/km (0.6 × 24 V/km) and occurred at approximately 5.4 seconds after detonation. To capture these characteristics in the model, ε(x,y) was uniform with a value set to 24 V/km, $\overline{e}(x, y)$ was uniform with a value of 90°, and the time-variation function, $f(t)$, was represented using the first 10 seconds of Figure 2-3.

E3B: Heave Wave

The E3B component used in this study was based on the environment described in [4]. The E3B wave was assumed to begin immediately after the blast-driven (E3A) component has subsided (at t=10 seconds) and continued until approximately 328 seconds after detonation. As with the E3A environment, the magnitude of the E3B electric field varied with time as illustrated in Figure 2-3, and the orientation remained fixed throughout the period associated with E3B. During the E3B time period ε(x,y) was modeled using the spatially varying function shown in Figure 2-5 and a function describing the spatial variation in electric field orientation, $\overline{e}(x, y)$. The spatial variation in electric field orientation was derived from Figure 2-6. During the E3B period, the peak electric field magnitude, 24 V/km, occurred at approximately 60 seconds. After t=198 seconds, the electric field decays and reaches zero at t=328 seconds. As described in [4] and [13], Figure 2-5 and Figure 2-6 are both oriented toward the earth's geomagnetic north pole

(as opposed toward the geographic north pole), a location that slowly varies with time. The location of the earth's geomagnetic north pole assumed for this study was 80.31° N, 72.62° W.

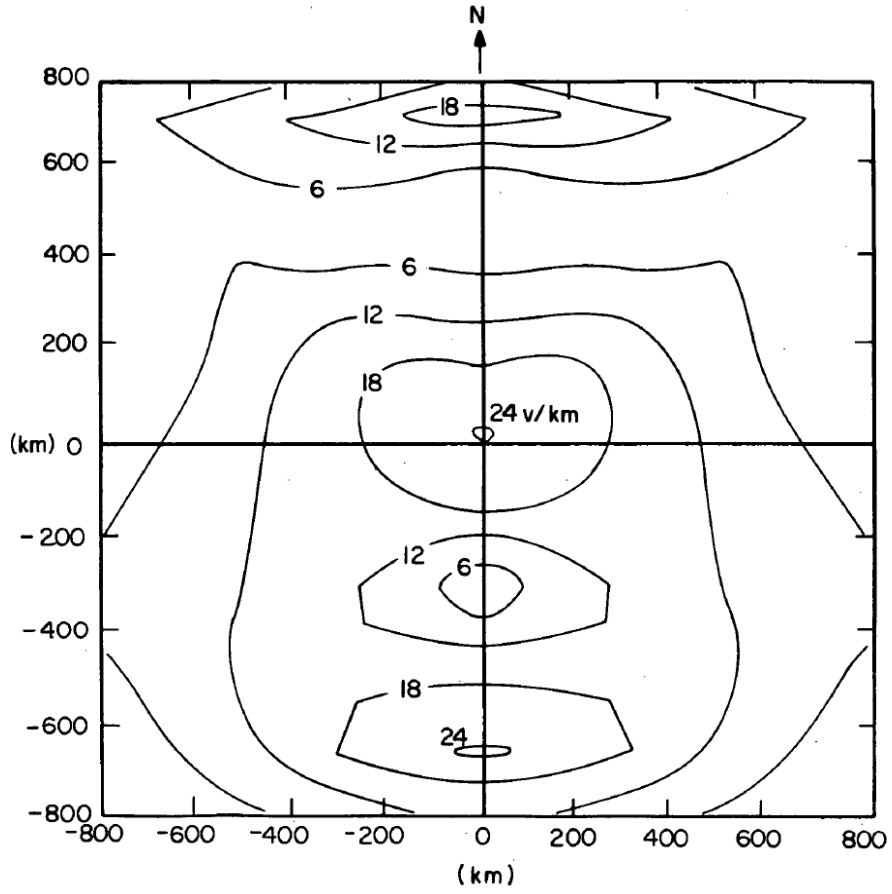

Figure 2-5
Spatially varying geoelectric field magnitude resulting from a detonation over the Central United States

Source: ORNL-6708 [4]

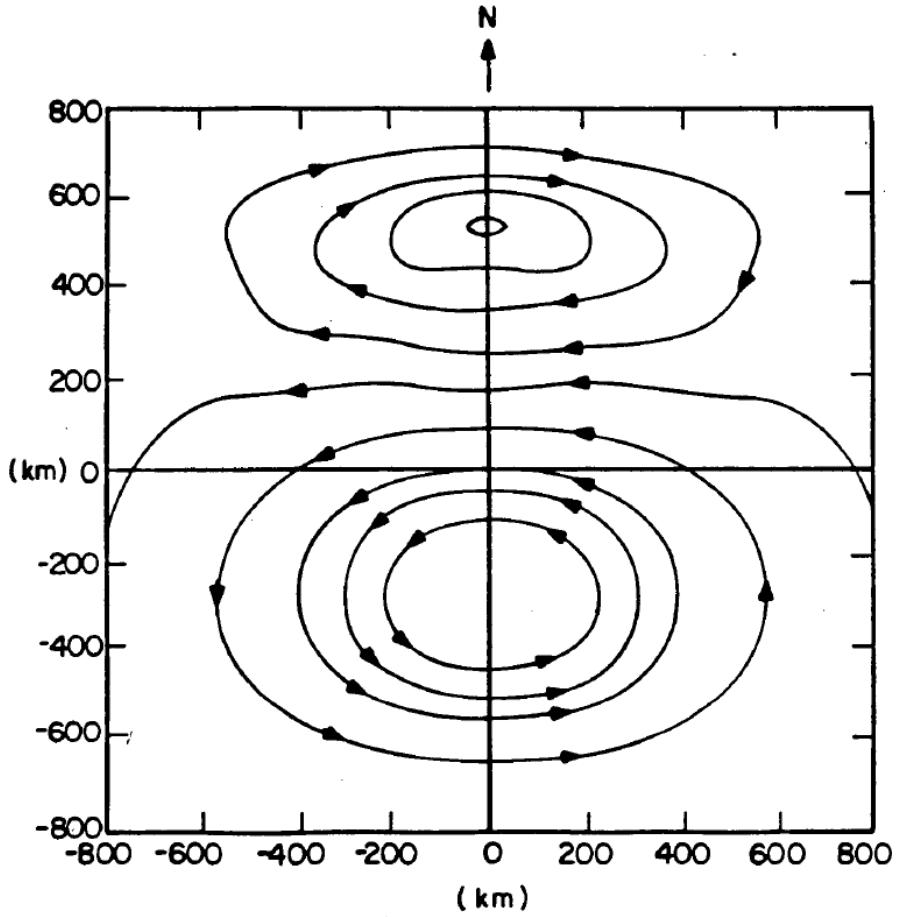

Figure 2-6
Spatially varying orientation of the geoelectric field resulting from a detonation over the Central United States

Source: ORNL-6708 [4]

In contrast to the uniform electric field associated with E3A, which can be reasonably assumed to cover an entire electrical interconnection, the E3B electric field is strongly dependent on the assumed geographic location of ground zero (target location). As an example, a contour map of the instantaneous geoelectric field at t=60 seconds (negative peak of the waveform shown in Figure 2-3) created by the previously described procedure for a target location in the CONUS is shown in Figure 2-7. The color bar to the right of the Figure 2-7 refers to the peak electric field (V/km).

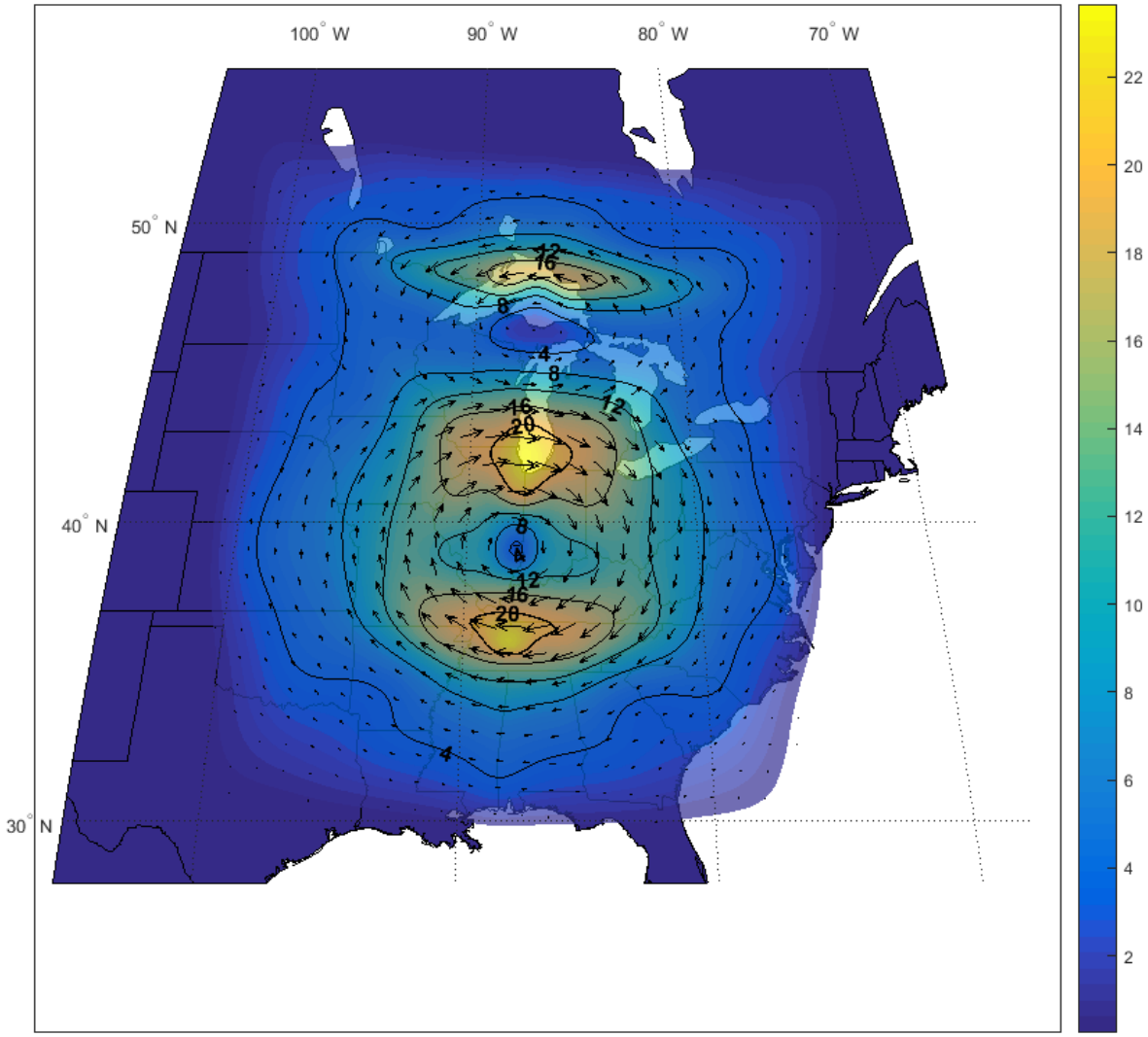

Figure 2-7
Geoelectric field at t=60 for detonation over a location in the Continental United States

For the purposes of this study, 11 target locations (ground zero locations) were evaluated. Target locations included areas in the Eastern Interconnection, the Western Interconnection, and the Texas Interconnection (ERCOT).

3
TRANSFORMER THERMAL ASSESSMENT

Overview

An assessment of the U.S. transformer fleet was performed to determine the potential for widespread transformer damage resulting from MHD-EMP (E3) from a single, high-altitude burst over the CONUS. The procedure that was followed to assess the U.S. transformer fleet is illustrated in Figure 3-1.

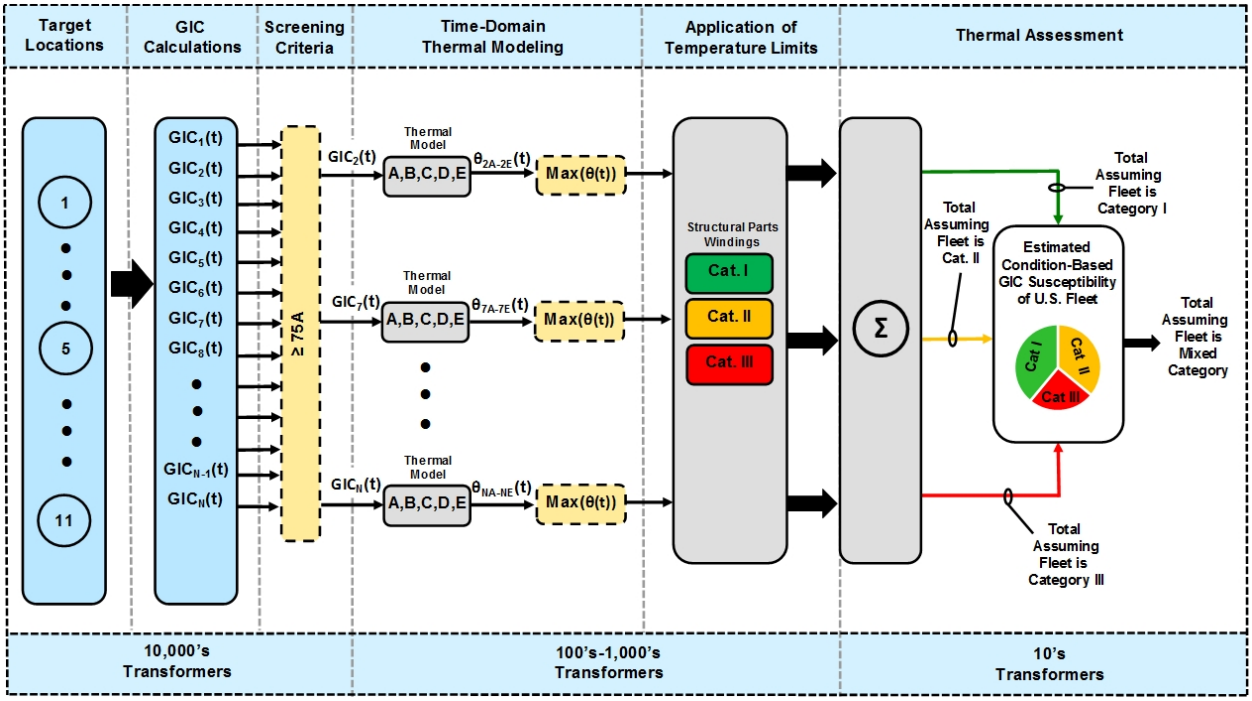

Figure 3-1
Procedure for performing assessment of U.S. transformer fleet

As shown in Figure 3-1, for each target location, the resulting time-series effective GIC flows were calculated for each bulk-power system transformer. For most target locations, this involved calculating GIC flows in tens of thousands of bulk-power system transformers. For some target locations, the GIC calculations involved bulk-power transformers in all three interconnections that were performed separately. Once the time-series GIC flows were computed, they were screened to determine which transformers experienced a peak instantaneous GIC level of 75 amps/phase or more. For the target locations considered, the number of transformers included in the thermal assessment, that is, those experiencing effective GIC flows of 75 amps/phase or more, was on the order of hundreds to a few thousand. A time-domain thermal analysis was then performed on all bulk-power system transformers experiencing 75 amps/phase or more of GIC. The results of the thermal analysis were then compared with conservative temperature limits to determine whether a given transformer would be at risk of possible thermal damage **if** the transformer was in the **assumed** condition-based GIC susceptibility category (that is, Category I,

Category II, or Category III). The number of transformers found to exceed the specified temperature limits was on the order of tens of transformers. The results of these calculations were then combined with results from an analysis that grouped U.S. transformers with operating voltages 230 kV or higher into the three categories of condition-based GIC susceptibility. Finally, the total number of transformers that would be at potential risk of thermal damage following a high-altitude nuclear burst with the MHD-EMP (E3) environment as described in Section 2 was estimated.

Geomagnetically Induced Current Analysis

The GIC calculations were performed in the time domain in order to provide the input data necessary to compute the hotspot temperature rise in the bulk-power transformers included in the model. Time-series GIC, $GIC(t)$, were computed for each element (transmission line or transformer) in the interconnection-wide model using the MHD-EMP (E3) environment described in Section 2. Because of modeling uncertainties and lack of specific transformer data, several conservative assumptions were made with regards to GIC modeling parameters. These are described in Section 2. Additional assumptions that were included in the GIC analysis are as follows:

- Only a single, high-altitude burst over a given target location was considered.
- The potential for E1 and E2 to damage protection and control equipment such that some transmission elements (transmission lines and transformers) could be removed from service immediately after detonation and prior to the creation of the MHD-EMP (E3) environment was not included in the analysis. Therefore, it was assumed, from a GIC calculation standpoint, that the effects of E1 or E2 would not result in changes to system topology or GIC flows.
- The potential voltage stability effects of E1, E2, and MHD-EMP (E3) were ignored in the GIC analysis. That is, the possibility of voltage collapse caused by E1, E2, or MHD-EMP (E3) and the resulting changes in system topology were ignored. This assumption is conservative because the reduction in GIC flows because of topological changes resulting from voltage collapse will tend to reduce hotspot heating in transformers.

Using these assumptions, time-series GIC calculations were carried out using interconnection-wide models for each of the 11 target locations. Of importance for transformer thermal simulations is the time-series effective GIC flow in transformers, which was computed for each 69 kV and above bulk-power transformer in the interconnection-wide model. When a target location affected more than one interconnection, the analysis of each affected interconnection was performed separately. As shown in Figure 2-3, the electric field (the source of the GIC) decays to zero at approximately 328 seconds. Therefore, if the effects of system inductance are ignored, the GIC will also decay to zero simultaneously. To fully simulate the effects of hotspot heating after the effects of MHD-EMP(E3) have dissipated, the resulting $GIC(t)$ waveforms were extended to 1200 seconds with amplitude of 0.0 amps/phase. Extending the $GIC(t)$ waveform beyond the 328 seconds point allowed for the observation of transformer cooling and the amount of time a given hotspot temperature limit was violated in cases in which the instantaneous hotspot temperature exceeded specified temperature limits.

Transformer Thermal Analysis

Once the GIC calculations were completed, a transformer thermal analysis was performed using the thermal model and modeling parameters described in Appendix A. As with GIC calculations, several conservative assumptions were made with regards to the thermal assessment, including the following:

- Half-cycle saturation of large power transformers was assumed to occur instantaneously, which provides a conservative estimate of hotspot heating.
- It was assumed that all transformers in the analysis could be described by one of the thermal models provided in Appendix A, and that at least one of the models would yield a hotspot temperature that would equal or exceed the level experienced during an actual event.
- The potential voltage stability effects of MHD-EMP (E3) were ignored in the thermal analysis. That is, the system voltage was assumed to remain near its pre-event value throughout the simulation period. In addition, the effects of harmonic voltage distortion were ignored. These assumptions regarding system voltage are conservative because a reduction in system voltage and/or harmonic voltage distortion tends to reduce the effects of half-cycle saturation, and hence, hotspot heating.
- Consistent with the procedure described in [14], the initial (pre-event) top oil temperature of all transformers in the analysis was assumed to be 80°C regardless of pre-event loading. Note: an initial top oil temperature of 80°C corresponds to an ambient temperature of 30°C (86°F) and transformer loading of approximately 0.84 per unit (pu) assuming a rated top oil rise of 65°C.
- Transformers experiencing effective GIC levels less than 75 amps/phase were assumed to be immune to thermal damage, which is consistent with the conservative approach adopted by the NERC [7, 14].
- In all transformer models, the asymptotic behavior of the transformer thermal response was assumed to be linear beyond 75 amps/phase of GIC. This assumption is conservative because the thermal response of transformers tends to saturate at higher values of GIC such as those considered in this study.

The procedure for determining transformer hotspot temperatures was based on the thermal response simulation approach described in NERC "Transformer Thermal Impact Assessment White Paper" [15]. The procedure that was used is as follows. First, the effective $GIC(t)$ waveform associated with every 69 kV and above transformer was screened, and a full transformer thermal time-series calculation was carried out for each transformer experiencing an instantaneous effective GIC value of 75 amps/phase or more. The thermal analysis was performed using each of the five thermal models (three models describing the hotspot temperature rise of structural parts and two models describing the hotspot rise in transformer windings) provided in Appendix A. Therefore, five separate time-series thermal simulations were performed for each bulk-power transformer experiencing an instantaneous effective GIC value of 75 amps/phase or more. An example of the simulated time-series hotspot temperatures using all five thermal models provided in Appendix A and the magnitude of the corresponding effective GIC flow is shown in Figure 3-2.

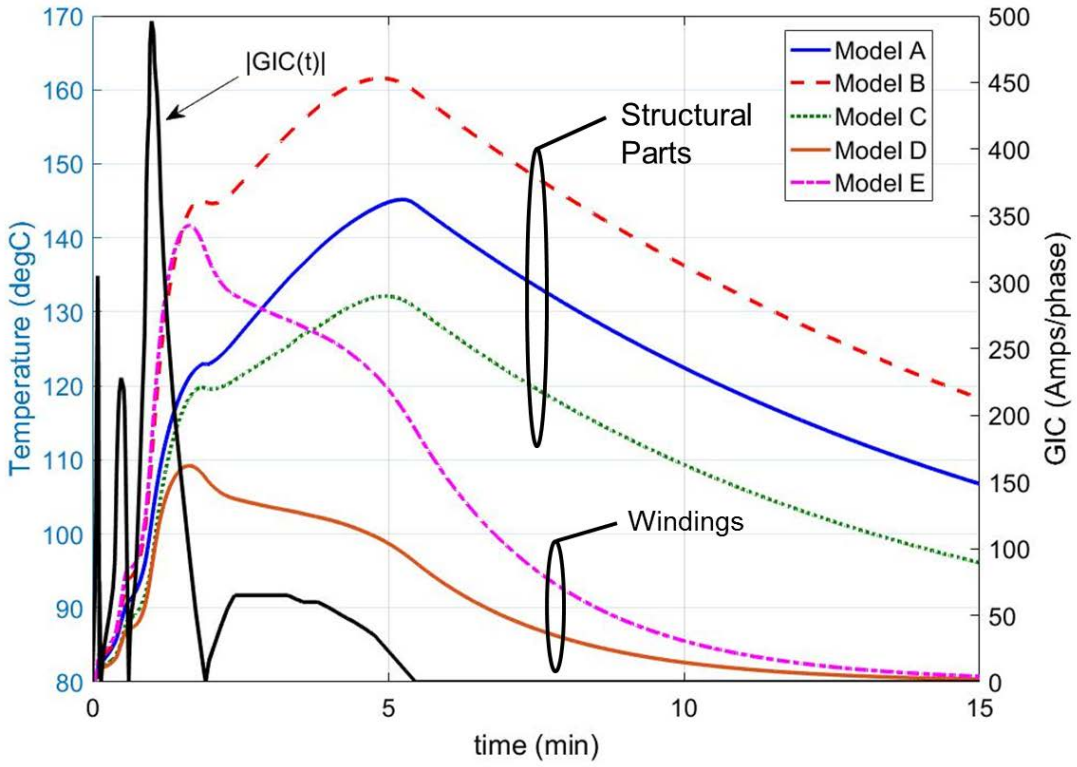

Figure 3-2
Example time-series hotspot temperature calculation results using all five thermal models

The time-series thermal calculation results of each transformer experiencing a peak effective GIC flow of 75 amps/phase or more were then used to inform the transformer fleet assessment.

Transformer Fleet Assessment

The last step in the assessment process was to utilize the time-series thermal calculation results to estimate the number of bulk-power transformers across the United States that could be at potential risk of thermal damage following a single, high-altitude nuclear detonation over the CONUS. First, suitable performance criteria or temperature limits were needed. NERC "Transformer Thermal Impact Assessment White Paper" [15] and IEEE Std. C57.163 [16] both provide conservative temperature limits; however, these limits assume that the transformers to be assessed are new [16]. Because not all transformers in the United States are new, temperature limits that accounted for condition-based GIC susceptibility were developed. The condition-based GIC susceptibility categories that the temperature limits were based are provided in Table 3-1.

Table 3-1
Criteria defining condition-based geomagnetically induced current susceptibility categories of transformers

Parameter	Condition-Based Geomagnetically Induced Current Susceptibility Category		
	I	II	III
Age	0–25	25–40	>40
Power Transformer Expert (PTX) software Abnormal Condition Code	1	2–3	4–5

As shown in Table 3-1, a combination of PTX Abnormal Condition Code and transformer age were used as criteria to determine condition-based GIC susceptibility of a given transformer. Note that in this specific context, "condition-based" refers to characteristics such as trends of dissolved gasses and age that are associated with the condition of a transformer and "GIC susceptibility" is related to potential vulnerabilities that may be exacerbated by a sudden increase in component temperatures that can occur during these events. The characteristics described in Table 3-1 are highly modified derivatives of those provided in Table 7-4 of the EPRI Copper Book [17]. The original table (that is, Table 7-4 of [17]) was intended to provide initial condition-based criteria for overloading of large power transformers and was designed to be utilized as a screening tool. Therefore, it is conservative by design, and as such, it is suitable for determining GIC susceptibility. The original table had four screening criteria: moisture, oxygen, ethylene, and ethane. For hotspot temperatures having extremely short duration such as those associated with GICs induced by MHD-EMP (E3), oxygen is not important because it is a factor in the acceleration of aging, which is minimal during these events. Ethane and ethylene were included as criteria in the original table to screen for units with potential incipient faults that would be exacerbated by overloads. The PTX Abnormal Condition Code [18], which is based on trends of ethylene and ethane, detects transformers with potential fault conditions that may be exacerbated by short-term heating such as that associated with GIC induced by MHD-EMP (E3). The PTX Abnormal Condition Code has been demonstrated to have a much lower false positive rate than simple thresholds on individual gases. Therefore, the PTX Abnormal Condition Code was used in lieu of the individual levels of ethane and ethylene that were provided in Table 7-4 of the EPRI Copper Book [17]. Moisture-in-paper is a critical parameter in the formation of bubbles during short-duration overloads. Unfortunately, it is difficult to differentiate moisture-in-paper (which cannot be measured directly) from moisture-in-oil (which can be measured). In lieu of using moisture-in-paper as a criterion, age can be used as a rough proxy. For extra-high-voltage transformers, maintenance practices are generally good and moisture content is kept low. However, as transformers age, moisture is generated, and there is an increasing likelihood of ingress from aged gaskets, and so on. Therefore, transformer age, while not absolute, is a reasonable proxy for estimating moisture content and was used in this study as a criterion for determining condition-based GIC susceptibility.

The temperatures limits provided in Table 3-2 were used as conservative screening criteria and refer to the condition-based GIC susceptibility categories provided in Table 3-1. For comparison, the hotspot temperature limits recommended in IEEE C57.163 [16] are 200°C and 180°C for structural parts and cellulose insulation (windings), respectively. It is important to note that exceeding the temperature limits provided in Table 3-2 does **not** suggest a high probability of

immediate failure; rather, it signals that the transformer may be at risk of potential thermal damage and that further analysis is needed using specific transformer design and operational data.

Table 3-2
Temperature limits based on condition-based geomagnetically induced current susceptibility categories

Condition-Based Geomagnetically Induced Current Susceptibility Category	Hotspot Temperature Limit	
	Structural Parts (°C)	Windings (°C)
I	180	160
II	160	140
III	140	120

The thermal assessment procedure was as follows. First, the maximum instantaneous hotspot temperature of each of the five thermal model outputs was determined for each transformer experiencing an instantaneous effective GIC flow ≥75 amps/phase. Next, the maximum instantaneous hotspot temperatures were then compared with the temperature limits shown in Table 3-2 assuming the following:

- All transformers were in **Category I.**
- All transformers were in **Category II.**
- All transformers were in **Category III.**

The total number of transformers that exceeded the temperature limits shown in Table 3-2 were then determined for each transformer model and category. For illustration purposes, the results of these calculations for Target Location 11 are provided in Table 3-3. The worst-case model results are also provided for each of the three categories. Note that the total number of transformers experiencing an effective GIC flow ≥75 amps/phase for this case was 1965 (not shown in Table 3-3).

Table 3-3
Total number of transformers exceeding temperature limits

Transformer Model	Model Type	Assumed Condition-Based Geomagnetically Induced Current Susceptibility Category		
		I	II	III
A	Structural part	0	0	10
B	Structural part	3	6	21
C	Structural part	0	0	4
D	Winding	0	0	0
E	Winding	1	6	28
Worst-case model results		**3**	**6**	**28**

Similar totals from this portion of the assessment for all 11 target locations are provided in columns 3 through 5 of Table 3-4.

Next, the condition-based GIC susceptibility category of U.S. bulk-power transformers was estimated using information from EPRI's transformer database and PTX software [18]. The analysis was limited to 1451 transformers with high-voltage windings rated 230 kV and above. Because data were not available to provide a more rigorous assessment of the moisture in paper for each of the 1451 transformers studied, age alone was used. The PTX Condition Codes and transformer age ranges provided in Table 3-1 were used as the basis for estimating the percentage of U.S. transformers in each category. The results of this analysis are provided in Figure 3-3.

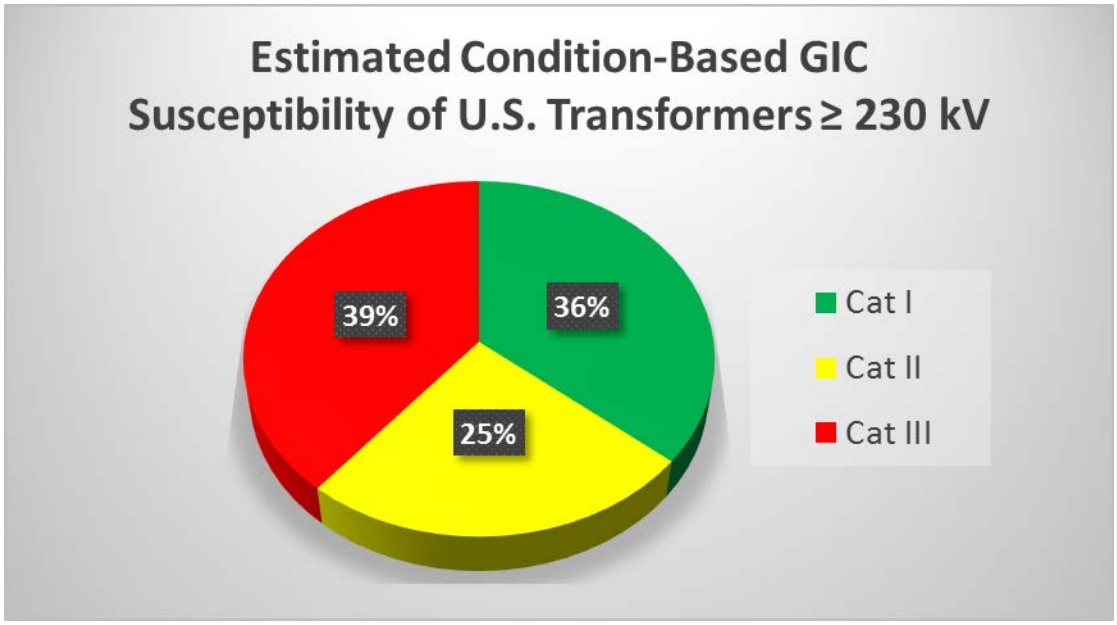

Figure 3-3
Estimated percentage of U.S. transformers operating at 230 kV or higher in each condition-based geomagnetically induced current susceptibility category

The values in Figure 3-3 represent, on average, the percentage of 230 kV and above bulk-power transformers in the United States that are in the specified category (combination of PTX Abnormal Code and age, refer to Table 3-1). An operating voltage of 230 kV and above was selected because a large percentage of transformers experiencing effective GIC flows of ≥75 amps/phase fell into this category. That said, it is important to recognize that the interconnection-wide model included transformers with operating voltages as low as 69 kV; however, the GIC flows in these transformers were found to be inconsequential. Because the data presented in Figure 3-3 are not specific to a given transformer, they may be interpreted in the following way. For any 230 kV and above transformer in the U.S. fleet, there is a 36% probability that it is in Category I, a 25% probability that it is in Category II, and a 39% probability that it is in Category III. Using the estimated percentages of transformers in each category and the total number of transformers exceeding the temperature limits in Table 3-2, assuming all transformers are of the same category, the expected number of transformers, $E(X)$, that would be at potential risk of thermal damage was determined using Equation 3-1:

$$E(X) = \sum_{j=1}^{K} p_j X_j$$
$$= p_1 X_1 + p_2 X_2 + p_3 X_3$$

Eq. 3-1

Where:

p_1 is the probability that a given transformer is in Category I

p_2 is the probability that a given transformer is in Category II

p_3 is the probability that a given transformer is in Category III

X_1 is the number of transformers exceeding the temperature limits assuming entire transformer fleet is in Category I

X_2 is the number of transformers exceeding the temperature limits assuming entire transformer fleet is in Category II

X_3 is the number of transformers exceeding the temperature limits assuming entire transformer fleet is in Category III

The results of this analysis are provided in Table 3-4.

Table 3-4
Number of transformers having a peak instantaneous GIC_{eff} ≥75 amps/phase and at risk of potential thermal damage

		Total Number of Transformers Exceeding Temperature Limits Based on Assumed Condition-Based Geomagnetically Induced Current Susceptibility of Entire Transformer Fleet			
Target Location	**Number of Transformers with GIC_{eff} ≥75 Amps/Phase**	**Category I**	**Category II**	**Category III**	**Mixed Category (I: 36%, II: 25%, III: 39%)**
1	1897	0	2	22	9
2	1872	2	4	15	8
3	1938	1	4	22	10
4	1912	2	6	19	10
5	1812	0	5	21	9
6	2435	0	3	15	7
7	689	0	2	10	4
8	692	0	1	7	3
9	675	2	3	11	6
10	2382	1	4	23	10
11	1965	3	6	28	14

Based on the analysis that was performed, it was found that of the tens of thousands of transformers that were included in the model evaluated for each target location, hundreds to thousands could experience effective GIC flows ≥75 amps/phase. However, of the hundreds to thousands of transformers that were then evaluated in more detail by performing a time-domain thermal analysis, only a small number of them were found to be at potential risk of thermal damage. To provide some context, for the worst-case target location, only 14 of the tens of thousands of transformers that were included in the model were found to be at potential risk of thermal damage. In addition, it was found that the transformers that were deemed at risk of potential thermal damage were geographically dispersed. That said, it is important to note that the potential impact of the loss of these transformers on system stability or time of restoration— should all of them experience immediate damage—was not considered in this study. Future analysis using location-specific information will be required to evaluate such potential effects.

The potential for thermal damage caused by circulating harmonic currents in the tertiary windings of large autotransformers was also evaluated. When the flow of GIC in the windings of the autotransformers results in half-cycle saturation, triplen harmonic currents can circulate in the tertiary winding resulting in additional hotspot heating. It was found that the level of circulating current is a nonlinear function of GIC, and at higher GIC levels when the transformer transitions from half-cycle saturation to full-cycle saturation, the circulating current is greatly diminished and tends toward zero. In addition, the short duration of the $GIC(t)$ generated by MHD-EMP (E3) plays a role in that the circulating current lasts on the order of 300 seconds. The transformer damage curves of IEEE C57.109 [19] indicate that large power transformers can withstand 3.0 pu current continuously for 300 seconds. None of the transformer designs investigated indicated a maximum effective tertiary current more than 3.0 pu, and the maximum effective tertiary current would last for only a short period (on the order of tens of seconds). Therefore, it was concluded that damaging levels of tertiary winding heating resulting from the flow of quasi-dc current generated by MHD-EMP (E3) are unlikely to occur, and as such, no additional analysis was included in this study. The details of this analysis are provided in Appendix B.

4
CONCLUSIONS

A detailed transformer thermal assessment using state-of-the-art modeling and analysis techniques was performed for the U.S. transformer fleet in order to determine the potential for widespread transformer damage caused by MHD-EMP (E3) from a single, high-altitude burst over the CONUS. Hotspot heating resulting from half-cycle saturation was evaluated for every bulk-power transformer included in each of the interconnection-wide models as well as the potential for thermal damage resulting from circulating harmonic current in the tertiary windings of large autotransformers. Based on the target locations that were evaluated and the assumed MHD-EMP (E3) environment presented in Section 2, it was determined that although a significant number of transformers (hundreds to thousands) could experience effective GIC flows greater than or equal to 75 amps/phase, only a small number of them would be at potential risk of thermal damage. In addition, the at-risk transformers were found to be geographically dispersed.

Although the analysis undertaken used the best available input data and state-of-the-art modeling techniques, uncertainties related to modeling parameters and the nature of the overall HEMP environment required that assumptions be made. These assumptions and their implications have been documented such that the results obtained can be used to inform mitigation measures and future assessments to determine the impacts of MHD-EMP (E3) on the bulk-power system. However, because of security concerns, specific information necessary to inform decisions at the utility level is not provided in this publicly available report. Such information will be provided as needed using the appropriate security protocols.

Finally, the analysis herein was based on a publicly available MHD-EMP (E3) environment that may or may not represent the environment generated during an actual HEMP attack. The potential effects of E1 and E2 prior to the generation of the MHD-EMP (E3) environment (for example, system topology changes because of protection and control system damage caused by E1 or E2) were also ignored because of a lack of understanding at the time of the analysis. Because of these uncertainties, it is not currently possible to place error bars around the analysis results. However, it is believed that because of the conservatism inherent in the assumptions that were made throughout the assessment process, the results presented provide a conservative estimate of the number of transformers that could be at potential risk of thermal damage caused by MHD-EMP (E3) resulting from a single, high-altitude burst of the CONUS. Although it was determined that a relatively small number of geographically dispersed transformers would be at potential risk of damage, the possible impact of the loss of these transformers on system stability or time of restoration—should all of them experience immediate damage—was not considered in this study. That said, it is important to recognize that identifying a transformer in this study as being at risk of potential thermal damage does not suggest a high probability of immediate failure. Rather, it signals that the transformer may be at risk of possible thermal damage and that further analysis is needed using information that is specific to a given transformer and system.

Future research efforts will focus on gaining a better understanding of the synergistic effects of E1, E2, and MHD-EMP (E3) and developing tools to include such effects in large-scale assessments such as the one presented in this report. In addition, future research efforts will seek to improve our understanding of the MHD-EMP (E3) environment and the overall system reliability impacts of experiencing damage to a small number of bulk-power transformers over a large area such as an electrical interconnection. Finally, it is recommended that this assessment be updated as information regarding HEMP impacts and improved modeling and analysis techniques become available.

5
REFERENCES

1. "Report of the Commission to Assess the Threat to the United States from Electromagnetic Pulse (EMP) Attack: Critical National Infrastructures," *The Commission to Assess the Threat to the United States from Electromagnetic Pulse*, 2008, http://www.empcommission.org/docs/A2473-EMP_Commission-7MB.pdf.
2. "Electromagnetic Pulse: Effects on the U.S. Power Grid, Executive Summary," *Metatech Corporation*, January 2010, https://www.ferc.gov/industries/electric/indus-act/reliability/cybersecurity/ferc_executive_summary.pdf.
3. "Meta-R-321, The Late-Time (E3) High-Altitude Electromagnetic Pulse (HEMP) and Its Impact on the U.S. Power Grid," *Metatech Corporation*, January 2010, https://www.ferc.gov/industries/electric/indus-act/reliability/cybersecurity/ferc_executive_summary.pdf.
4. J.R. Legro, N.C. Abi-Samra, F. M. Tesche, "Study to Assess the Effects of Magnetohydrodynamic Electromagnetic Pulse (HEMP) on Electric Power Systems – Phase I – Final Report," *Oak Ridge National Laboratory*, 1985, Accessed February 7, 2017, http://web.ornl.gov/info/reports/1985/3445600437392.pdf
5. F.M. Tesche, E.F. Vance, "Electromagnetic Pulse Research on Electric Power Systems: Program Summary and Recommendations," *Oak Ridge National Laboratory,* 1993, Accessed February 7, 2017. http://web.ornl.gov/info/reports/1993/3445605662155.pdf
6. L. Marti, "Simulation of Transformer Hotspot Heating Due to Geomagnetically Induced Currents," *IEEE Transactions on Power Delivery,* Vol. 28, No. January, pp. 320–327, 2013.
7. "TPL-007-1 Transmission System Planned Performance During Geomagnetic Disturbances," *North American Electric Reliability Corporation (NERC)*, Atlanta, GA, 2016, http://www.nerc.com/_layouts/PrintStandard.aspx?standardnumber=TPL-007-1&title=Transmission%20System%20Planned%20Performance%20for%20Geomagnetic%20Disturbance%20Events&jurisdiction=United%20States.
8. "Application Guide: Computing Geomagnetically-Induced Current in the Bulk-Power System," *North American Electric Reliability Corporation (NERC),* 2013, http://www.nerc.com/comm/PC/Geomagnetic%20Disturbance%20Task%20Force%20GMDTF%202013/GIC%20Application%20Guide%202013_approved.pdf
9. *Geomagnetic Disturbance Vulnerability Assessment and Planning Guide.* EPRI, Palo Alto, CA: 2016. 3002008358.
10. T. J. Overbye, "Power Grid Sensitivity Analysis of Geomagnetically Induced Currents," *IEEE Transactions on Power Systems,* Vol. 28, No. 4, pp. 4821–4828, 2013.
11. K. Zheng, "Effects of System Characteristics on Geomagnetically Induced Currents," *IEEE Transactions on Power Systems,* Vol. 29, No. 2, pp. 890–898, 2014.
12. *Investigation of Geomagnetically Induced Currents in the Proposed Winnipeg-Duluth-Twin Cities 500 kV Transmission Line, EL-1949.* EPRI, Palo Alto, CA: 1981.

13. G. B. Rackliffe, “Simulation of Geomagnetic Currents Induced in a Power System by Magnetohydrodynamic Electromagnetic Pulses,” *IEEE Transactions on Power Delivery,* Vol. 3, No. 1, pp. 392-397, 1988.
14. “Screening Criterion for Transformer Thermal Impact Assessment,” *North American Electric Reliability Corporation (NERC)*, October 2014, Accessed February 7, 2017, http://www.nerc.com/pa/Stand/Project201303GeomagneticDisturbanceMitigation/GMD_Thermal_screening_Oct27_clean.pdf
15. “Transformer Thermal Impact Assessment White Paper,” *North American Electric Reliability Corporation (NERC)*, December 2014, Accessed February 7, 2017, http://www.nerc.com/pa/Stand/Project201303GeomagneticDisturbanceMitigation/thermal_impact_assessment_whitepaper_Dec5_clean.pdf
16. *Guide for Establishing Power Transformer Capability While Under Geomagnetic Disturbances,* IEEE Standard C57.163-2015.
17. *EPRI Power Transformer Guidebook: The Copper Book.* EPRI, Palo Alto, CA: 2010. 3002005902.
18. *PTX Transformer Fleet Management Software, version 3.0.* EPRI, Palo Alto, CA: 2016. 3002007833.
19. *Guide for Liquid-Immersed Transformers Through-Fault Duration,* IEEE Standard C57.109-1993.
20. J. E. M. Lahtinen, “GIC Occurrences and GIC Test for 400 kV System Transformer,” *IEEE Transactions on Power Delivery,* Vol. 17, No. 2, pp. 555-561,2002.
21. K. V. R. Girgis, “Effects of GIC on Power Transformers and Power Systems,” *IEEE Transmission and Distribution Conference,* Orlando, FL, 2012.
22. C. K. R. Girgis, “Calculation Techniques and Results of Effects of GIC Currents as Applied to Two Large Power Transformers,” *IEEE Transactions on Power Delivery,* Vol. 7, No. 2, pp. 699-705,1992.
23. International Electrotechnical Commission 61000-2-9, “Electromagnetic Compatibility (EMC)–Part 2: Environment, Section 9: Description of HEMP Environment–Radiated Disturbance,” International Electrotechnical Commission, Geneva, Switzerland, 1996.
24. *Analysis of Geomagnetic Disturbance (GMD) Related Harmonics.* EPRI, Palo Alto, CA: 2014. 3002002985.
25. *Recommended Practice for Establishing Transformer Capability When Supplying Nonsinusoidal Load Currents,* IEEE Standard C57.110-2008.
26. *Guide for Loading Mineral-Oil-Immersed Transformers*, IEEE Standard C57.91-2011

A
TRANSFORMER THERMAL MODEL

Overview

This appendix describes the theoretical basis of the time-domain thermal model that was developed and used in the assessment and the way that the parameters for each of the five thermal models that were used in the assessment were determined. In addition, this appendix provides the results of the simulations that were used to validate the models.

Model Development

Measurement data have shown that the hotspot temperature rise, $\Delta\theta_{HS}(t)$ of a power transformer experiencing half-cycle saturation because of the flow of dc current in its windings increases exponentially (see Figure A-1).

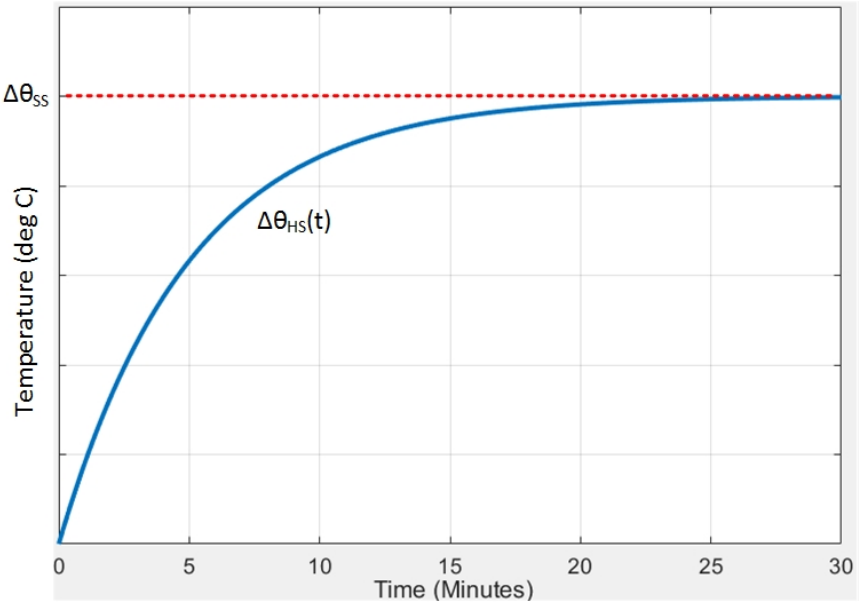

Figure A-1
Example hotspot temperature rise of a power transformer injected with dc current

Assuming that the data shown in Figure A-1 can be described by a single exponential, the hotspot temperature rise can be described mathematically as:

$$\Delta\theta_{HS}(t) = \Delta\theta_{SS}\left(1 - e^{-\frac{t}{\tau}}\right) \qquad \textbf{Eq. A-1}$$

Where:

$\Delta\theta_{HS}(t)$ is the hotspot rise (°C)
$\Delta\theta_{SS}$ is the steady-state hotspot rise corresponding to a specific dc current level (°C)
τ is the thermal time constant (seconds) of the component being evaluated (for example, transformer winding, tie plate, and so on)

Because injecting a transformer with dc current is equivalent to applying a step function, Equation A-1 can be considered the step response. The unit step response, $g(t)$, can be obtained by per-unitizing Equation A-1 using the dc current level, i_{dc}, that was used to establish the original step response, that is:

$$g(t) = \frac{\Delta\theta_{SS}}{i_{dc}}\left(1 - e^{-\frac{t}{\tau}}\right) \qquad \textbf{Eq. A-2}$$

The unit impulse response, $h(t)$, can then be obtained by taking the derivative of the unit step response with respect to time:

$$h(t) = \frac{dg}{dt} = \frac{\Delta\theta_{SS}}{\tau\, i_{dc}} e^{-\frac{t}{\tau}} \qquad \textbf{Eq. A-3}$$

It is convenient to cast Equation A-3 into the form shown in Equation A-4, where $K = \Delta\theta_{SS}/i_{dc}$.

$$h(t) = K\left\{\frac{1}{\tau} e^{-\frac{t}{\tau}}\right\} \qquad \textbf{Eq. A-4}$$

The s-domain unit impulse response can be described by:

$$H(s) = K\left\{\frac{1}{1+\tau\, s}\right\} \qquad \textbf{Eq. A-5}$$

The s-domain transfer function described in Equation A-5 can be converted to its z-domain equivalent using the bilinear transformation:

$$s = \frac{2}{\Delta t}\left(\frac{1-z^{-1}}{1+z^{-1}}\right) \qquad \textbf{Eq. A-6}$$

where Δt is the time step (seconds). Substituting Equation A-6 into Equation A-5 and solving for $H(z)$ results in Equation A-7:

$$H(z) = K\left\{\frac{1}{1+\tau\cdot s}\right\}\Bigg|_{s=\frac{2}{\Delta t}\left(\frac{1-z^{-1}}{1+z^{-1}}\right)} = K\cdot\left\{\frac{1+z^{-1}}{\left(1+\frac{2\tau}{\Delta t}\right)+\left(1-\frac{2\tau}{\Delta t}\right)z^{-1}}\right\} \qquad \textbf{Eq. A-7}$$

Using Equation A-7, convolution in the *z*-domain can be performed using Equation A-8:

$$Y(z) = X(z)H(z) \qquad \textbf{Eq. A-8}$$

Where:

$X(z)$ is an arbitrary input
$Y(z)$ is the corresponding output

For programming purposes, it is convenient to cast Equation A-8 in the form of a difference equation as shown in Equation A-9:

$$y(k+1) = \left(\frac{K}{1+\frac{2\tau}{\Delta t}}\right)\left(x(k+1)+x(k)\right) - \left(\frac{1-\frac{2\tau}{\Delta t}}{1+\frac{2\tau}{\Delta t}}\right)y(k) \qquad \textbf{Eq. A-9}$$

The variable K has been described previously as a constant; however, this assumption is not strictly valid. The asymptotic behavior of large power transformers experiencing half-cycle saturation has been shown to be nonlinear [6, 16]. This effect can be accommodated in the model using a look-up table based on nonlinear asymptotic behavior of the transformer, and is implemented in Equation A-9 by computing K at each time step as indicated by $K(k)$ in Equation A-10:

$$y(k+1) = \left(\frac{K(k)}{1+\frac{2\tau}{\Delta t}}\right)\left(x(k+1)+x(k)\right) - \left(\frac{1-\frac{2\tau}{\Delta t}}{1+\frac{2\tau}{\Delta t}}\right)y(k) \qquad \textbf{Eq. A-10}$$

It is also important to recognize that the thermal time constant is typically different for the heating mode and the cooling mode. The transformer is assumed to be in the heating mode when the input $x(k+1)$ is greater than or equal to the value of the previous time step, $x(k)$. The transformer can be assumed to be in the cooling mode when the input $x(k+1)$ is zero or less than the value of the previous time step, $x(k)$.

To determine the total hotspot temperature, THS, the hotspot rise computed using Equation A-10 is added to the top oil temperature, θ_{TO}:

$$THS(k+1) = \theta_{TO} + y(k+1) \qquad \textbf{Eq. A-11}$$

Because the time constant of the oil is on the order of hours, the top oil temperature can be assumed constant during the short period associated with MHD-EMP (E3).

Model Parameters

The following sections describe the way that the parameters for each of the five thermal models that were used in the assessment were determined, as well as provide the results of the simulations used to validate the models.

Transformer Model A (Structural Part)

Simulations using a finite element method (FEM) model were performed by the manufacturer of a 133.3 megavolt ampere (MVA) 230kV:115kV:13.2kV autotransformers (400 MVA three-phase bank rating) to determine the effects of half-cycle saturation on hotspot heating. For simulation purposes, the transformer was connected to a fictitious strong grid, and various levels of dc current were injected into the neutral of the autotransformer with the X terminals open circuited. The transformer was assumed unloaded during the simulations. The maximum hotspot temperature recorded during the simulations was located on the core tie plate and is provided in Figure A-2.

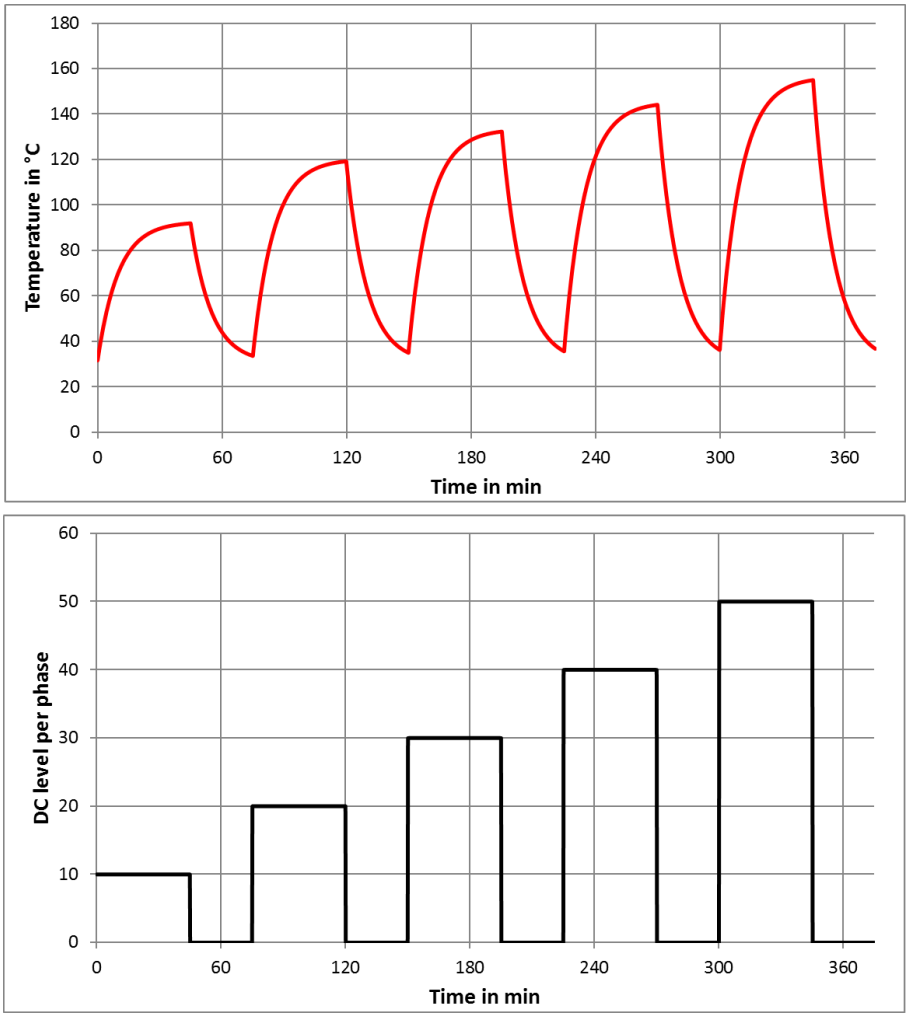

Figure A-2
Maximum simulated hotspot temperature in tie plate corresponding to five dc current levels

The simulated temperatures shown in Figure A-2 were used as the basis of Transformer Model A. The asymptotic behavior of the model is provided in Table A-1. Note that asymptotic values beyond 50 amps/phase are based on the slope of a straight-line segment describing the last two entries in the table.

Table A-1
Asymptotic behavior of Transformer Model A (Structural Part)

Geomagnetically Induced Current (amps/phase)	Steady-State Temperature Rise (°C)
10	62
20	90
30	103
40	115
50	126
5000	5571

The heating time constant was chosen to be 600 seconds, and the cooling time constant was chosen to be 650 seconds. A comparison of the results based on Equation A-11 and the FEM simulations performed by the transformer manufacturer is provided in Figure A-3.

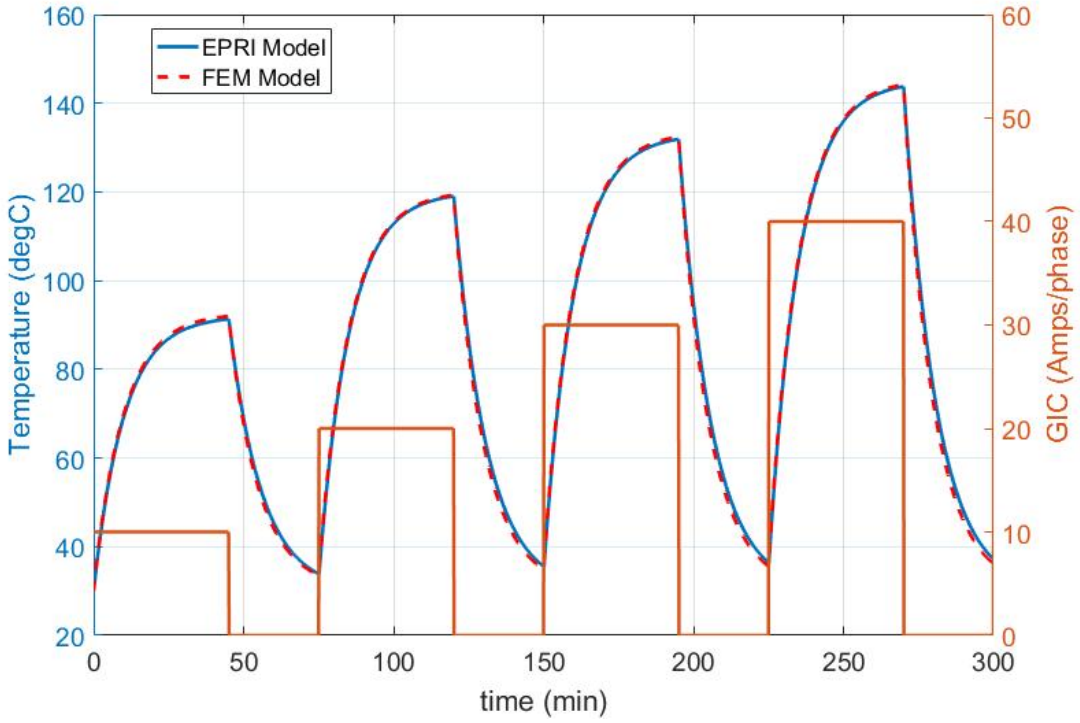

Figure A-3
Transformer Model A: comparison of EPRI model and finite element method simulation results of structural part hotspot temperature for five dc current levels

Transformer Model B (Structural Part)

Transformer B is defined in [6] as a single-phase 133 MVA 500kV:16.5kV transformer (400 MVA three-phase bank rating). During a factory acceptance test, the transformer was energized at nominal voltage and injected with 5 amps of dc current. The corresponding hotspot temperature rise of the core tie plate was measured. Winding hotspot temperature data were not provided.

The measured hotspot temperature corresponding to a dc current injection of 5 amps/phase is provided in [6]. The thermal time constant for the Transformer B model was found to be 780 seconds for the heating phase. No information regarding the thermal time constant during the cooling phase was provided in [6]; therefore, the cooling time constant was also assumed to be 780 seconds. Additional information necessary to derive the asymptotic behavior was not provided; therefore, a linear asymptotic behavior was assumed. The slope of the straight-line segment representing the asymptotic behavior was 2.76°C/amp. A comparison of the simulated hotspot temperature rise using the thermal model described in Equation A-11 and the measured hotspot temperature rise is provided in Figure A-4.

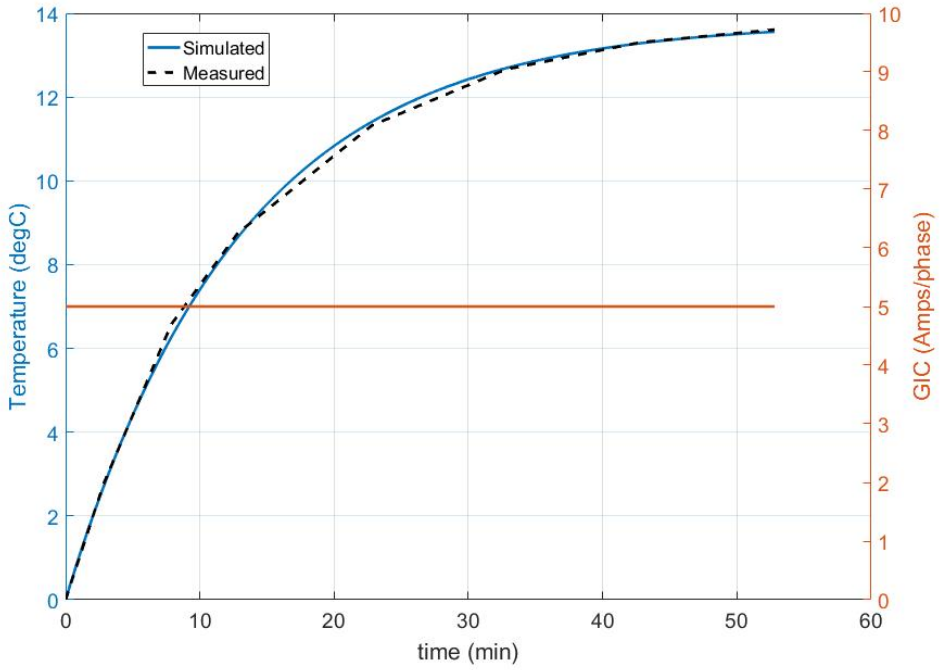

Figure A-4
Transformer Model B: comparison of EPRI model and measured hotspot temperature of Transformer B tie plate

Transformer Model C (Structural Part)

Transformer C is described in [20] as a three-phase 410 kV:120kV:21 kV GY-GY-D 400 MVA three-winding transformer. During a field test, the transformer was energized at nominal voltage and injected with various levels of dc current, and the corresponding hotspot temperatures were measured at various locations within the transformer. See Figure 8 in [20] for further details regarding the hotspot temperature measurements.

The thermal model associated with this study was based on the highest measured temperature. The asymptotic behavior is provided in Table A-2. The asymptotic behavior beyond 67 amps/phase was assumed linear.

Table A-2
Asymptotic behavior of Transformer Model C (Structural Part)

Geomagnetically Induced Current (amps/phase)	Steady-State Temperature Rise (°C)
17	36
27	54
33	65
42	78
50	90
59	100
67	114
5000	5403

The heating time constant was chosen to be 800 seconds, and the cooling time constant was chosen to be 500 seconds. A comparison of the simulated hotspot temperature rise and the measured hotspot temperature rise is provided in Figure A-5.

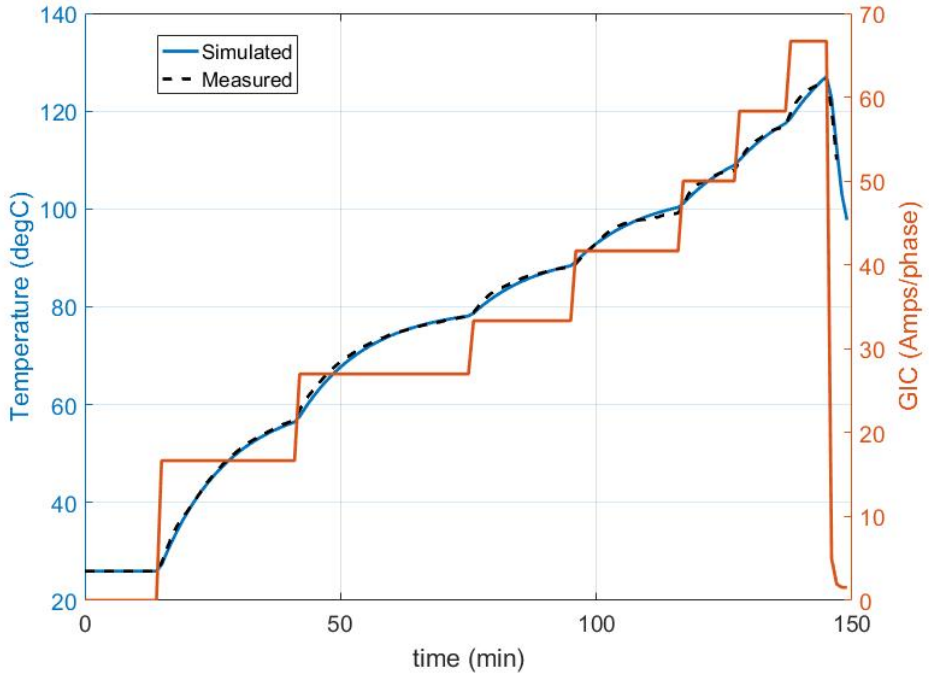

Figure A-5
Transformer Model C: comparison of EPRI model and measured hotspot temperature of transformer tie plate

Transformer Model D (Winding)

Transformer D is described in [6] as a single-phase 250 MVA 345kV:24.5kV conventional transformer (750 MVA three-phase bank rating). The simulated data provided in [21] were fitted with a single exponential in [6]. The thermal time constant was found to be 150 seconds. No information regarding the thermal time constant during the cooling phase was provided in [6] or [21]; therefore, the cooling time constant was assumed to be 150 seconds. The asymptotic behavior was based on the temperature rise associated with a GIC level of 20 amps/phase and was assumed linear with a slope of 0.3°C/amp. A comparison of the model and simulated data are provided in [6].

Transformer Model E (Winding)

Transformer E is described in [22] as a single-phase generator step-up unit (GSU) rated 433 MVA 418.8kV:20.5kV (1299 MVA three-phase bank rating). The maximum temperature rise above the ambient oil temperature for this transformer carrying 60 amps/phase of GIC was calculated to be 38°C for the high-voltage coils and 7°C for the low-voltage coils using a time-domain model of the transformer consisting of magnetic and electrical circuits and a 3D field/loss program [22]. Because no data were provided, the thermal time constants for heating and cooling were assumed to be the same as those of Transformer D or 150 seconds. The model used in this study was based on the high-voltage coil data; therefore, the asymptotic behavior was assumed linear with a slope of 38/60°C/amp or 0.63°C/amp. Time-domain data suitable for model comparison were not provided in [22].

B
COMPARISON OF MAGNETOHYDRODYNAMIC ELECTROMAGNETIC PULSE WAVESHAPE ON TRANSFORMER HOTSPOT HEATING

An important input parameter of a transformer thermal assessment is the wave shape of the GIC that flows in the windings of a given transformer. An analysis was performed to compare the hotspot heating that would result from the International Electrotechnical Commission (IEC) 61000-2-9 [23] wave shape and the ORNL wave shape (Figure 2-3) that was used in the assessment. For comparison, it was assumed that the resulting GIC(t) would be similar in shape to the electric field waveform, and both were scaled to provide a peak amplitude of 1000 amps/phase. The resulting time-series hotspot temperature was simulated using the worst-case structural part model (Transformer Model B). The initial temperature of the structural part was assumed to be 80°C. The results of the thermal simulations are provided in Figure B-1.

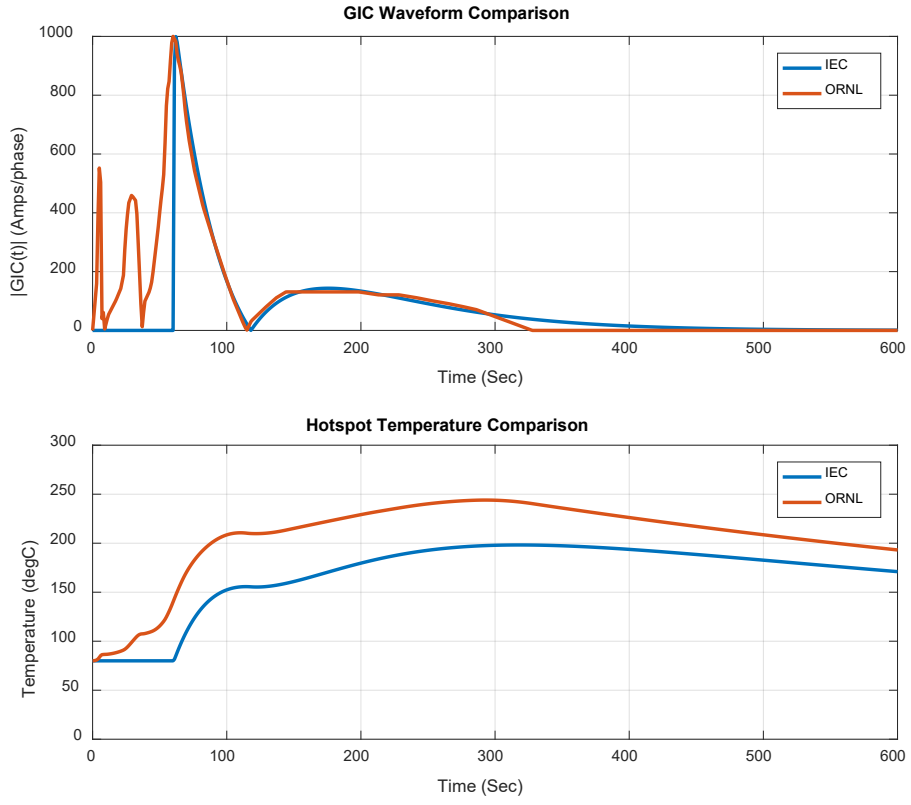

Figure B-1
Comparison of simulated hotspot temperatures using International Electrotechnical Commission and Oak Ridge National Laboratory geomagnetically induced current wave shapes

Referring to Figure B-1, the maximum hotspot temperature associated with the ORNL waveform is approximately 248°C as compared with approximately 198°C obtained using the IEC waveform. Therefore, it can be concluded that the ORNL waveform provides a conservative estimate of the hotspot heating relative to the IEC waveform.

C
ANALYSIS OF GEOMAGNETICALLY INDUCED CURRENT IMPACTS ON AUTOTRANSFORMER DELTA TERTIARY WINDINGS

Overview

This appendix describes a study that was performed to determine the potential risk of thermal damage caused by circulating currents in the tertiary windings of large autotransformers. The overall approach to this investigation was to perform an electrical analysis to calculate the transformer exciting currents and the portion of the exciting currents circulating in the delta tertiary winding, and then assess the thermal impact of the resulting tertiary current.

Electrical Analysis

The fundamental and harmonic exciting current components of a transformer, energized by an ac source and simultaneously subjected to direct current flow, can be directly calculated by the analytical expressions documented in [24]. These analytical expressions are valid only for banks of single-phase transformers and are strictly valid only if a delta winding is not present. This is because the circulating flow of zero-sequence current in the delta winding partially shields the transformer core from the magnetomotive force (mmf) of the main winding. To determine the delta winding flow and the transformer saturation performance, a reasonable transformer model must be used.

For this analysis, a conventional "T" equivalent model was used, as illustrated in Figure C-1 in per-unit format. A T equivalent model is usable only for a two-winding transformer. Only two windings of the autotransformer need to be considered in this analysis, the H (series + common) and T (tertiary) windings, because it is assumed that the dominant ac voltage source is applied only to the H terminals. From transformer test reports, the leakage impedance from the H to T terminals (X_{HT}) is defined. The air-core impedances of the H and T windings (X_{acH} and X_{acT}) can also be determined or estimated. The X_H, X_T, and X_{ac} parameters of the T equivalent model allow three variables to match the three known transformer impedances.

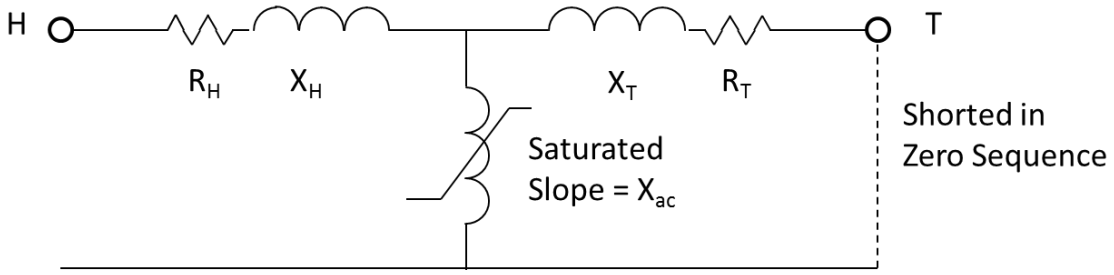

Figure C-1
"T" equivalent transformer model

X_{ac} is the fully saturated slope of the nonlinear inductance element of the T model (times $2\pi \cdot 60$). A typical magnetizing current (excitation current at rated flux) is modeled as well a typical curved transition from the unsaturated to saturated state. The unsaturated magnetizing current, curvature, and saturation level parameters, however, have very little impact on the results where deep saturation from the quasi-dc current is involved.

The H terminal of the T model is connected to an ideal 60 Hz voltage source. The T terminal is open for positive and negative sequence currents and is short circuited by the delta connection for zero-sequence currents. The current of the nonlinear element flows through the linear inductances of the model, affecting the voltage and flux waveforms at the midpoint node to which the nonlinear element is connected. Positive and negative sequence currents flow only through X_H, and zero-sequence currents flow through the parallel combination of X_H and X_T. The current through the X_T element represents the circulating current in the delta tertiary winding and is determined by the current division of the total nonlinear element current.

In the specific case of a bank of identical single-phase transformers, energized by an ideal positive-sequence (that is, balanced) fundamental voltage source at the terminals, the zero-sequence current is exclusively triplens (harmonics with orders that are integer multiples of three), and triplen components are exclusively zero sequence. It should be noted that this is not the case if three-phase transformers (such as shell-form and five-leg core-form) are involved, nor is it an accurate assumption if the voltage applied to the transformer is not purely positive sequence (that is, unbalanced).

Because of the very long time that constants are involved in dc-offset saturation, time-domain simulation by electromagnetic transient programs can be unwieldy. Therefore, an iterative analysis approach, which combines time-domain and frequency-domain analysis, was used.

A flux offset level that provides a dc component of exciting current equal to the desired value was determined using Equations 2 and 3 of [24]. An initial estimate of the excitation current fundamental and harmonic current components was made using Equations 5 and 6 of [24]. These harmonic and fundamental currents were injected into the center node of the T equivalent model (node where the nonlinear branch in Figure C-1 is connected), and the resulting voltage spectrum was determined. The voltage spectrum was transformed to the time domain and applied to the nonlinear element to determine a new current estimate. This current waveform was transformed back to the frequency domain, and the iterative process was continued until convergence.

Much of the analysis was performed considering currents up to the 42nd harmonic in the frequency domain and 500 points per cycle (33.3 μs increments) in the time-domain analyses. A sensitivity case was run with 10,000 points per cycle (1.66 μs increments) and up to the 100th harmonic without significant change of the salient results.

Transformer Thermal Analysis

The primary objective of the investigation is the evaluation of the circulating delta currents and their potential thermal impact. The magnitudes and spectral contents of the delta currents were evaluated to determine the tertiary winding hotspot temperature impact by adaptation of formulas provided in IEEE C57.110 [25]. The harmonic currents were related to an equivalent fundamental-frequency current that can be compared with the transformer overcurrent damage curves provided in IEEE C57.109 [19], which assume fundamental-frequency current.

Because of their harmonic content, the tertiary currents during asymmetric saturation have an increased heating effect relative to a fundamental-frequency current of equal rms magnitude. Transformer-series losses (losses that result from current flow through the winding, in contrast with excitation losses) are composed of real power losses that are proportional to the square of the rms current magnitude and are frequency invariant, and stray losses that depend on both current magnitude and frequency. Stray losses are composed of winding eddy current losses and "other stray losses" that occur outside of the winding (such as leakage flux impinging on core clamps and causing eddy losses). All losses contribute to the bulk oil heating, but only real power and winding eddy losses contribute to the temperature rise of the winding above the oil temperature. Because the thermal time constant of oil temperature rise above ambient is on the order of 4 hours or more, and MHD-EMP (E3) events are of relatively short duration (less than 5 minutes), oil temperature rise can be ignored. The critical issue is the winding hotspot temperature rise that has a time constant on the order of a few minutes.

IEEE C57.110 [25] defines harmonic loss factors for winding eddy and other stray losses. The eddy winding eddy current harmonic loss factor is the ratio of eddy current power loss for the distorted winding current divided by the power loss for fundamental-frequency current of the same rms magnitude. Eddy current power loss at each harmonic frequency is in proportion to the squares of both the current magnitude I_h and the harmonic order h. Therefore, the calculation of the winding eddy harmonic loss factor F_{HL}, for a given current spectrum, is shown in Equation C-1.

$$F_{HL} = \frac{\sum_{h=1}^{h\max} (I_h \cdot h)^2}{\sum_{h=1}^{h\max} I_h^{\,2}} \qquad \textbf{Eq. C-1}$$

At the hottest spot of a winding, the temperature rise θ_{HS} above the top oil temperature is given in Equation C-2, where θ_{HS_r} is the hotspot temperature rise at rated conditions (rated undistorted current I_{rated}), I_{rms} is the rms magnitude of the distorted winding current, m is an empirical exponent, and K_{EC} is the ratio of eddy current loss density divided by the total loss density (eddy plus ohmic losses) at the hotspot location.

$$\theta_{HS} = \theta_{HS\_r} \cdot \left[\frac{I_{rms}^{\,2} \cdot \left[(1 - K_{EC}) + F_{HL} \cdot K_{EC} \right]}{I_{rated}^{\,2}} \right]^m \qquad \textbf{Eq. C-2}$$

The empirical exponent m is set to 0.8 in IEEE C57.110 [19], based on the recommendations of IEEE C57.91 [26], which indicates that the empirical exponent m is used, in part, to account for changes in oil viscosity with temperature that affect heat transfer from the winding to the oil. Both standards are concerned with long-term or steady-state loading conditions in which convective heat transfer is important. The duration of an MHD-EMP (E3) event, however, is sufficiently short that heating of the winding is mostly adiabatic. Therefore, this analysis uses an exponent of unity to conservatively reflect this different situation.

Defining I_{eff} as the effective fundamental current that yields the same hotspot temperature rise, Equation C-3 can be written and then simplified and solved for I_{eff} as shown in Equation C-4.

$$\theta_{HS\_r} \cdot \left[\frac{{I_{eff}}^2 \cdot \left[(1 - K_{EC}) + \cdot K_{EC} \right]}{{I_{rated}}^2} \right]^1 = \theta_{HS\_r} \cdot \left[\frac{{I_{rms}}^2 \cdot \left[(1 - K_{EC}) + F_{HL} \cdot K_{EC} \right]}{{I_{rated}}^2} \right]^1 \quad \textbf{Eq. C-3}$$

$$I_{eff} = I_{rms} \cdot \sqrt{(1 - K_{EC}) + F_{HL} \cdot K_{EC}} \quad \textbf{Eq. C-4}$$

The short-term overcurrent limits specified in the transformer damage curves in IEEE C57.109 [19] can then be used to evaluate the magnitude and duration of the effective current.

Example Transformer

This investigation has been performed using a specific large autotransformer as an example. The relevant transformer test data are listed in Table C-1. In addition, some physical parameters of the transformer that allowed estimation of the tertiary winding's air-core impedance were available.

Table C-1
Transformer test data

Parameter	Value	Units
Main-winding rating (self-cooled by natural convection)	80	MVA
Tertiary winding rating (self-cooled by natural convection)	14	MVA
Rated voltage (H terminal, series + common winding)	132.8	kV
Rated voltage (L terminal, common winding)	66.4	kV
Rated voltage (tertiary winding)	13.2	kV
High-voltage winding resistance (series + common) at 85°C	0.12146	Ω
Tertiary winding resistance at 85°C	0.013916	Ω
Leakage impedance (H − T) at nominal tap	38.08	Ω
Measured load loss (H − L) at nominal tap at 85°C	74.09	kW at 602.5 A
Measured load loss (H − T) at nominal tap at 85°C	56.2	kW at 175.5 A
Saturated slope of saturation curve	0.833	%/%
Flux-axis intercept of saturated slope	1.2	per unit (pu)

Thermal Parameters

The load loss and winding dc resistance test data allowed estimation of the tertiary winding eddy current loss factor K_{EC}. First, the H to L winding dc resistance and load-loss test power results were used to determine the stray losses in this test:

$$74.09 \times 10^3 - 602.5^2 \cdot 0.1246 = 28860 \text{ W} \qquad \textbf{Eq. C-5}$$

Based on the recommendation of IEEE C57.110 [19], 33% of this stray loss is assumed to be a result of winding eddy currents. The ratio of the eddy current loss divided by resistive loss is:

$$\frac{0.33 \cdot 28.86 \times 10^3}{602.5^2 \cdot 0.1246} = 0.21 \qquad \textbf{Eq. C-6}$$

Because of the 2:1 ratio of the autotransformer main winding, it can be reasonably assumed that the stray loss factor is approximately equal for both the series and common windings. This ratio will be used in a following step, in which the main and tertiary winding stray losses found in the H-T load-loss tests are segregated by winding.

The total stray losses in the H − T load-loss test are:

$$56.2 \times 10^3 - 175.5^2 \cdot 0.1246 - \left(\frac{132.8}{13.2} \cdot 175.5 \right)^2 \cdot 0.013916 = 8980 \text{ W} \qquad \textbf{Eq. C-7}$$

Of these stray losses, 33% are assumed to be winding eddy losses, or 2.963 kW. The main-winding eddy losses in this test are estimated, using the factor calculated in Equation C-6, to be:

$$175.5^2 \cdot 0.1246 \cdot 0.21 = 806 \text{ W} \qquad \textbf{Eq. C-8}$$

Therefore, the stray loss of the tertiary winding in this test is 2963 − 806 W, or 2157 W. The average ratio of this tertiary winding eddy loss divided by the tertiary winding losses (sum of the ohmic and eddy losses) is:

$$\frac{2157}{\left(\frac{132.8}{13.2} \cdot 175.5 \right)^2 \cdot 0.013916 + 2157} = 0.0474 \qquad \textbf{Eq. C-9}$$

This ratio is the average eddy current factor over the tertiary winding. However, eddy current heating is unevenly distributed. IEEE C57.110 [25] recommends that the eddy current factor at the winding hot spot should be assumed to be 400% of the average value. Therefore, the tertiary winding eddy current factor K_{EC} used in Equation C-4 for determining effective winding current is 0.189.

Impedance Parameters

The transformer T equivalent model was constructed in per unit on the main winding's natural convection base. The leakage reactance X_{HT} is 0.3808 pu, as documented in the transformer test report. The main-winding air-core reactance, determined from the slope of the saturation curve provided by the manufacturer, is 0.833 pu. This value is extraordinarily large for a core-form

transformer; however, the base used for the percent current in this saturation curve was not documented. If it is assumed to be on the full second stage forced cooling (ONAF2) rating, then the air-core reactance equates to 0.502 pu on the ONAN base, which is well within the typical range for core-form transformers. Therefore, the latter per-unit value was used.

The manufacturer's test data did not include a saturation curve measured from the tertiary terminals. However, data were available indicating that the area of the core is 0.40 m^2 and the magnetic length of the core is 7.84 m. The tertiary winding has 72 turns. If it is assumed that the winding height is 50% of the core length, and the area of the winding is 150% of the core area (considering stepping of the core, winding cylinder, and insulation space), the inductance of the winding is estimated to be 988 μH. This equates to 0.372 Ω, or 0.171 pu on the main-winding ONAN MVA base and the tertiary winding voltage base.

The values of the T equivalent model were calculated as follows:

$$X_H = \frac{X_{HT} + X_{acH} - X_{acT}}{2} = \frac{0.3808 + 0.502 - 0.171}{2} = 0.3559 \qquad \textbf{Eq. C-10}$$

$$X_T = \frac{X_{HT} + X_{acT} - X_{acH}}{2} = \frac{0.3808 + 0.171 - 0.502}{2} = 0.0249 \qquad \textbf{Eq. C-11}$$

$$X_{ac} = \frac{X_{acH} + X_{acT} - X_{HT}}{2} = \frac{0.502 + 0.171 - 0.3808}{2} = 0.1461 \qquad \textbf{Eq. C-12}$$

The H branch winding resistance is 0.00055 pu, and the T branch winding resistance is 0.00639 pu. These resistances have negligible impact on the results.

The transformer described here is labeled "Design 1." In addition to this set of transformer parameters, two additional sets of parameters were chosen for evaluating parametric sensitivity. It is common practice for users of transient simulation tools to connect the saturation branch to the lowest-voltage terminals. This results in X_T being zero and represents a severe case for delta tertiary circulating currents because of saturation. Design 2 is an adjustment of the Design 1 parameters to achieve this condition. Shell form transformers have substantially larger air-core reactance than typical core-form transformers. In addition, because of the interleaved pancake-type windings, there is no inner or outer winding, and the air-core reactance of the windings are closer to each other in per-unit magnitude. Design 3 represents an estimation of shell form transformer characteristics. The reactance of the three designs is summarized in Table C-2.

Table C-2
Transformer impedance parameters

Design	X_{HT} (per unit)	X_{acH} (per unit)	X_{acT} (per unit)	X_H (per unit)	X_T (per unit)	X_{ac} (per unit)
1	0.381	0.502	0.171	0.356	0.025	0.146
2	0.380	0.500	0.120	0.380	0.000	0.120
3	0.380	1.000	0.800	0.290	0.090	0.710

Analysis Results

Tertiary currents, in per unit of the tertiary winding's base, are plotted in Figure C-2 for a wide range of dc current values. Both the rms and effective current values are shown. At dc levels exceeding the peak ac voltage divided by the transformer's air-core impedance seen from the energized terminal (X_{acH}), the transformer is fully saturated for the entirety of each cycle. Therefore, the transformer exciting current is exclusively fundamental frequency (assuming that the applied ac voltage is undistorted fundamental) and positive sequence. Therefore, there is ideally no current circulating in the delta when the dc current exceeds this threshold. In the case of the parameters assumed for Design 1, this critical full-cycle saturation threshold is 1704A.

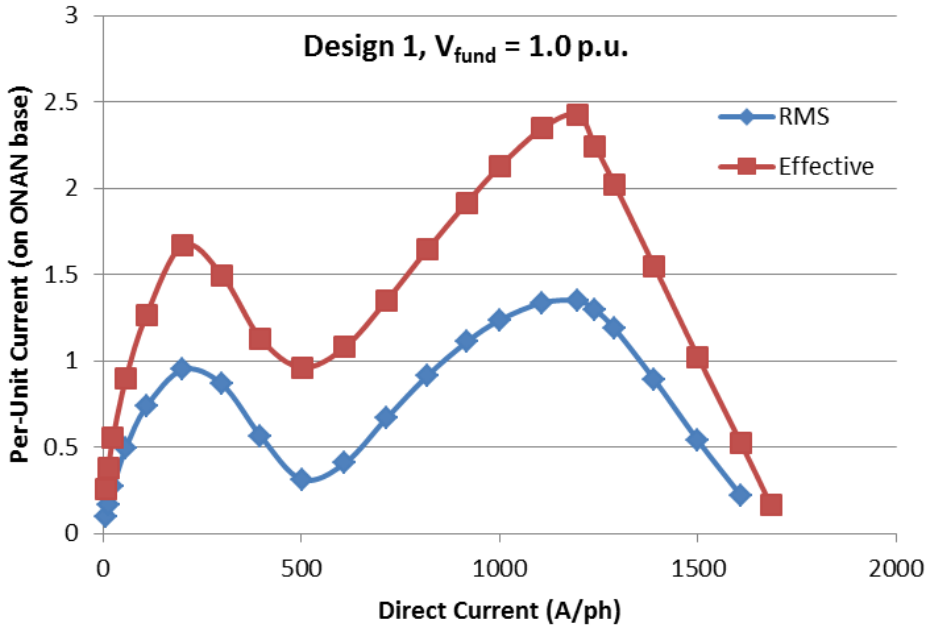

Figure C-2
Delta tertiary current as a function of direct current for transformer Design 1 parameters at 1.0 pu fundamental voltage

The wave shapes of the main winding (H), tertiary winding (T), and total exciting current of the transformer model's nonlinear branch are shown in Figure C-3 for a dc current level of 1000 amps/phase.

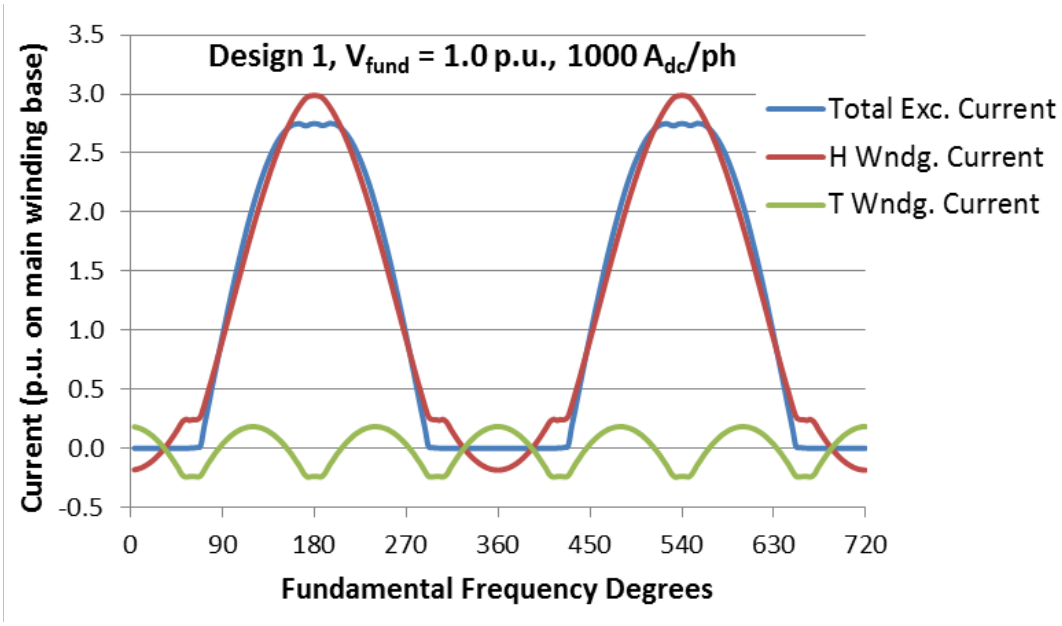

Figure C-3
Current wave shapes for transformer Design 1 at 1.0 pu fundamental voltage and 1000 amps/phase dc current (per-unit base is on the main winding ONAN rating)

The contributions of individual harmonic components to winding heating are related to the product of the current magnitude times the harmonic order. Figure C-4 shows the harmonic current components up to the 99th order, weighted by the harmonic order, for a dc magnitude of 1000 amps/phase. Because the components' impacts are combined by root sum square (refer to Equations C-1 and C-4), the lowest order harmonics tend to have the largest weights and dominate the thermal impact. Figure C-5 plots the effective current and the lowest two zero-sequence harmonic components (third and sixth). The effective current magnitude variations are well correlated to the third harmonic. Note that the sixth harmonic current component shows cyclic variations as the dc increases ("beating").

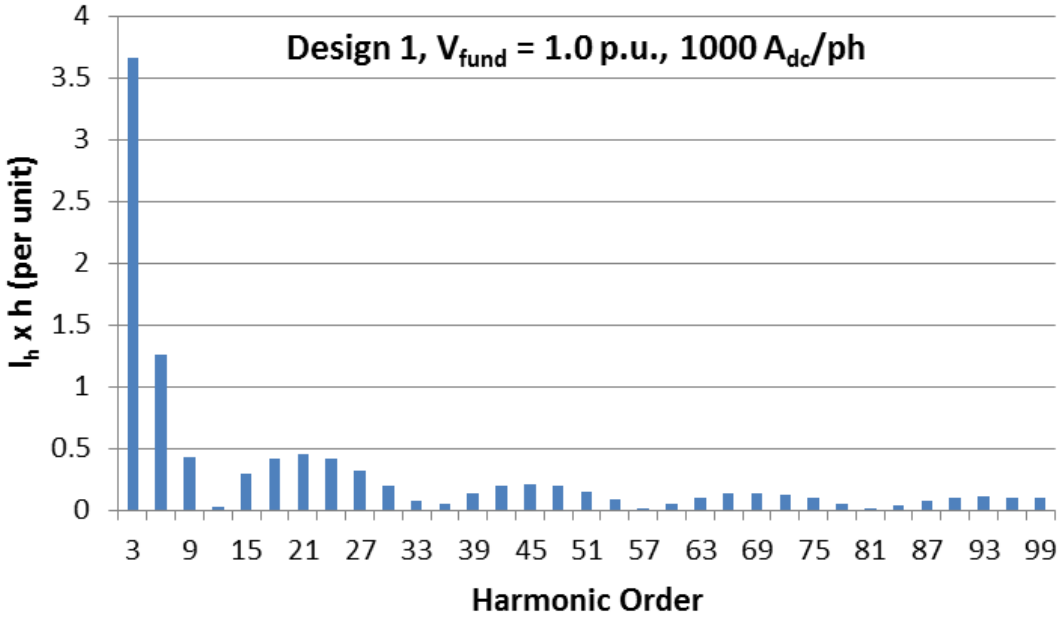

Figure C-4
Product of delta tertiary current harmonic components times the harmonic order at direct current of 1000 amps/phase for transformer Design 1 parameters at 1.0 pu ac voltage

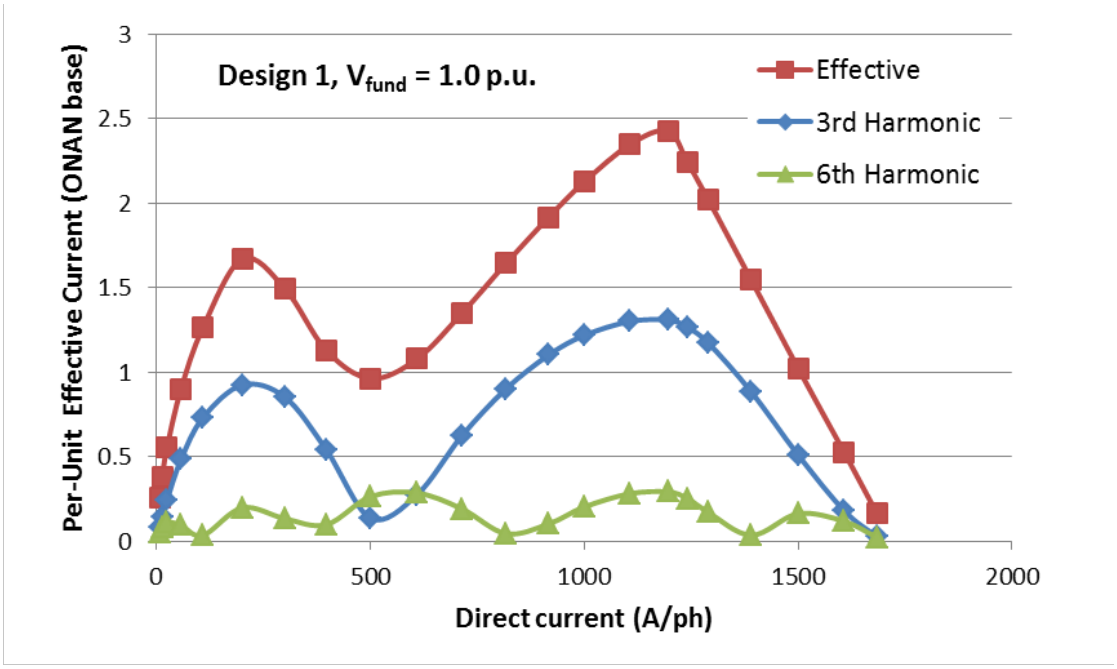

Figure C-5
Delta tertiary current components as a function of direct current for transformer Design 1 at 1.0 pu fundamental voltage

With large dc currents forced through transformers, the fundamental voltages at the terminals are likely to be severely depressed because of the very large amount of reactive power absorbed by transformers throughout the system. Figure C-6 shows that for a dc current level of 1000 amps/phase, the effective heating value of the circulating delta tertiary current decreases rapidly with decreasing fundamental voltage. At 0.589 pu fundamental voltage, 1000 amps of dc causes the transformer to be in full-cycle saturation, and the delta tertiary current is zero. At 500 amps/phase of dc (refer to Figure C-7) in which the delta current versus direct current curve is near a local minimum, the impact of reduced fundamental voltage is very different. By calculation, the fundamental voltage in which full-cycle saturation occurs for 500 amps/phase of dc is 0.295 pu, well below the level at which the power system can remain stable.

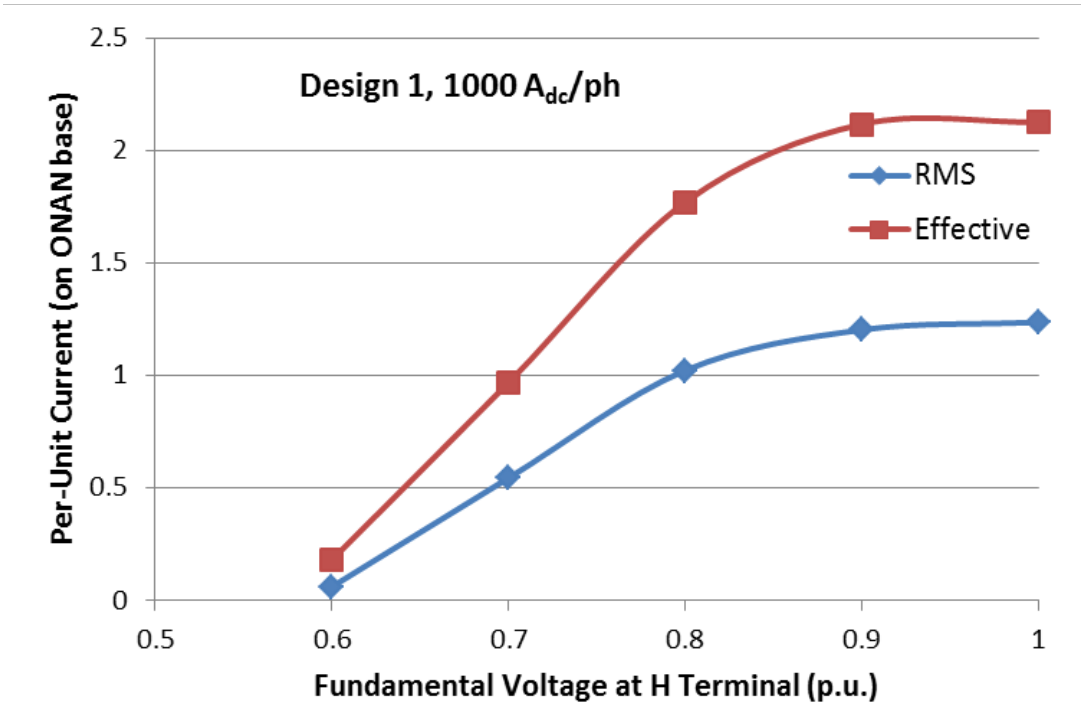

Figure C-6
Delta tertiary current components as a function of fundamental-frequency voltage for transformer Design 1 parameters at 1000 amps/phase of direct current

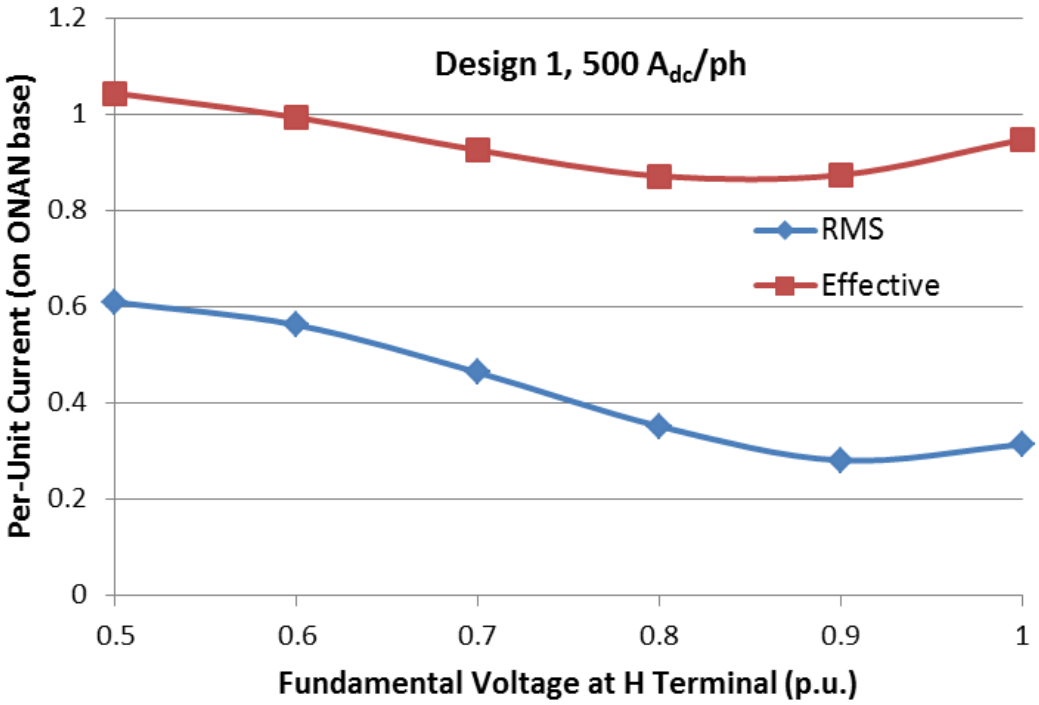

Figure C-7
Delta tertiary current components as a function of fundamental-frequency voltage for transformer Design 1 parameters at 500 amps/phase of direct current

The three transformer "designs" are compared in Figure C-8. Design 3, which is assumed to be typical of shell form transformers, experiences far less tertiary winding thermal impact from the dc saturation.

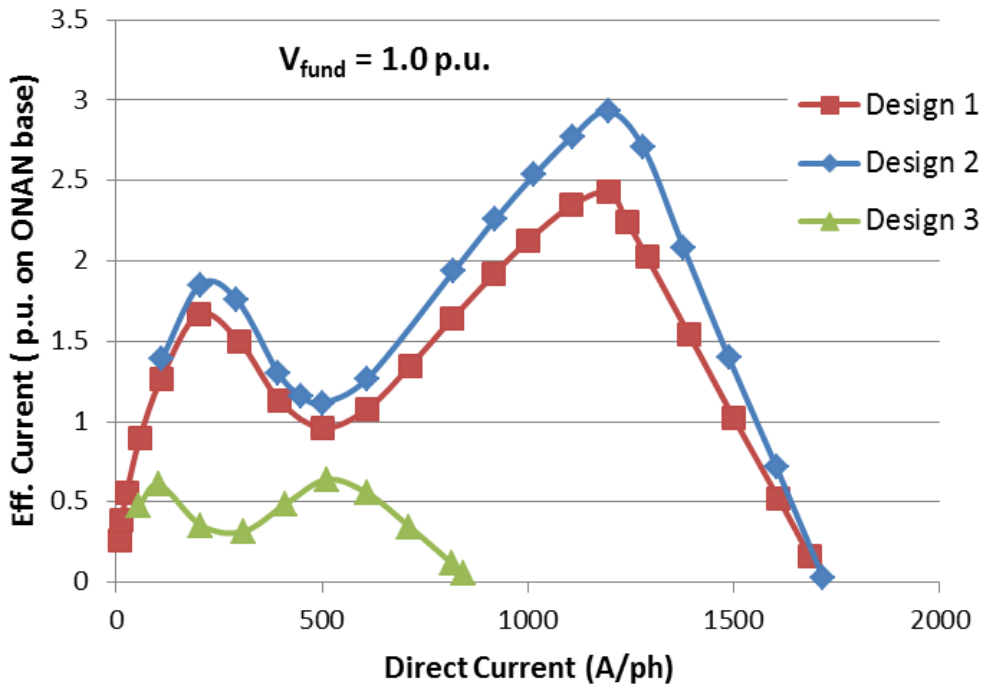

Figure C-8
Effective tertiary current versus direct current for three transformer designs

Thermal Impact Evaluation

The reference MHD-EMP (E3) electric field wave shape used in the subject study is illustrated in Figure 2-3. It can be assumed that the wave shape of the quasi-direct current in transformers during a HEMP event would follow a similar wave shape (see Figure 2-3), with perhaps some attenuation of the peak due to occurring during an actual event because of power system inductance, which was not modeled in this study. The duration of this wave is on the order of 300 seconds long, and the magnitude of direct current during most of this period is a small fraction of the peak. The transformer damage curves of IEEE C57.109 [19] indicate that a Category IV (large power) transformer should withstand a continuous 3 pu current for 300 seconds. None of the transformer designs investigated indicate a maximum possible effective tertiary current in excess of 3 pu. Therefore, GICs induced by MHD-EMP (E3) and not lasting for longer than those evaluated in this study (that is, 328 seconds) should not cause damaging tertiary winding heating. This conclusion, however, is based on the ratio of main to tertiary winding MVA ratings of the example transformer, which is considered typical. Transformers with larger MVA ratios require further investigation, considering their impedances.

Conclusions

The following are the major conclusions reached in this investigation:

- For the transformer parameters considered in this investigation, quasi-direct currents generated by MHD-EMP (E3) are unlikely to cause damaging tertiary winding heating.
- Transformers with larger ratios of main-to-tertiary-winding MVA rating than considered in this investigation (5.7:1) may have tertiary winding vulnerability, but further study using actual impedance data for such transformers is necessary in order to make a determination.
- Transformers having increased air-core impedance, as seen from the ac-energized terminals, have less circulating currents in the delta tertiary. The minimum main-winding air-core impedance considered in this investigation is 0.5 pu. Transformers with lower air-core impedance may have tertiary winding vulnerability, but further study using actual impedance data for such transformers is necessary in order to make a determination.
- At direct current magnitudes exceeding the crest ac voltage divided by the air-core reactance seen from the energized terminal, the transformer is saturated continuously throughout each cycle. The resulting exciting current is fundamental frequency and does not have a zero-sequence component (under idealized conditions), and therefore, does not cause any delta winding current.
- The maximum effective delta tertiary winding current occurs at approximately 70% of the GIC level that results in full-cycle saturation.
- For direct current magnitudes causing high effective tertiary circulating currents, the magnitude of the effective tertiary current decreases rapidly with decrease in the fundamental voltage applied to the transformer.

The Electric Power Research Institute, Inc. (EPRI, www.epri.com) conducts research and development relating to the generation, delivery and use of electricity for the benefit of the public. An independent, nonprofit organization, EPRI brings together its scientists and engineers as well as experts from academia and industry to help address challenges in electricity, including reliability, efficiency, affordability, health, safety and the environment. EPRI members represent 90% of the electric utility revenue in the United States with international participation in 35 countries. EPRI's principal offices and laboratories are located in Palo Alto, Calif.; Charlotte, N.C.; Knoxville, Tenn.; and Lenox, Mass.

Together…Shaping the Future of Electricity

3002009001

Electric Power Research Institute
3420 Hillview Avenue, Palo Alto, California 94304-1338 • PO Box 10412, Palo Alto, California 94303-0813 • USA
800.313.3774 • 650.855.2121 • askepri@epri.com • www.epri.com